AGU PUBLICATIONS

Paleoceanography

RESEARCH ARTICLE
10.1002/2017PA003146

Unraveling the onset of Cretaceous Oceanic Anoxic Event 2 in an extended sediment archive from the Tarfaya-Laayoune Basin, Morocco

Wolfgang Kuhnt[1], Ann E. Holbourn[1], Sebastian Beil[1], Mohamed Aquit[1,2], Tim Krawczyk[1], Sascha Flögel[3], El Hassane Chellai[4], and Haddou Jabour[5]

[1]Institute of Geosciences, Christian-Albrechts-University, Kiel, Germany, [2]Direction de Recherche et Développement, Recherche Géologique, OCP S.A., Youssoufia, Morocco, [3]Ozeanzirkulation und Klimadynamik, Paläo-Ozeanographie, GEOMAR Helmholtz-Zentrum für Ozeanforschung Kiel, Kiel, Germany, [4]Department of Geology, Faculty of Sciences Semlalia, Cadi Ayyad University, Marrakech, Morocco, [5]ONHYM, Office National des Hydrocarbures et des Mines, Rabat, Morocco

Abstract We investigated the onset and development of Cretaceous Oceanic Anoxic Event 2 (OAE2) in a newly drilled core (SN°4) from the Tarfaya Basin (southern Morocco), where this interval is unusually expanded. High-resolution (centimeter-scale equivalent to centennial) analysis of bulk organic and carbonate stable isotopes and of carbonate and organic carbon content in combination with XRF scanner derived elemental distribution reveal that the ocean-climate system behaved in a highly dynamic manner prior to and during the onset of OAE2. Correlation with the latest orbital solution indicates that the main carbon isotope shift occurred during an extended minimum in orbital eccentricity (~400 kyr cycle). Shorter-term fluctuations in carbonate and organic carbon accumulation and in sea level related terrigenous discharge were predominantly driven by variations in orbital obliquity. Negative excursions in organic and carbonate $\delta^{13}C$ preceded the global positive $\delta^{13}C$ shift marking the onset of OAE2, suggesting injection of isotopically depleted carbon into the atmosphere. The main $\delta^{13}C$ increase during the early phase of OAE2 in the late Cenomanian was punctuated by a transient plateau. Maximum organic carbon accumulation occurred during the later part of the main $\delta^{13}C$ increase and was associated with climate cooling events, expressed as three consecutive maxima in bulk carbonate $\delta^{18}O$. The extinctions of the thermocline dwelling keeled planktonic foraminifers *Rotalipora greenhornensis* and *Rotalipora cushmani* occurred during the first and last of these cooling events and were likely associated with obliquity paced, ocean-wide expansions, and intensifications of the oxygen minimum zone, affecting their habitat space on a global scale.

Key Points:
- The onset of OAE2, which corresponds to a two-stepped increase in $\delta^{13}C$ spanning ~100 kyr, is preceded by negative carbon isotope excursions
- A three-stepped transient climate cooling with intermittent brief anoxic episodes occurred in the latest stage of the main $\delta^{13}C$ increase
- Two major extinction events of thermocline dwelling planktonic foraminifers were closely linked to intensifications of the OMZ

Supporting Information:
- Supporting Information S1
- Data Set S1

Correspondence to:
W. Kuhnt,
wk@gpi.uni-kiel.de

Citation:
Kuhnt, W., A. E. Holbourn, S. Beil, M. Aquit, T. Krawczyk, S. Flögel, E. H. Chellai, and H. Jabour (2017), Unraveling the onset of Cretaceous Oceanic Anoxic Event 2 in an extended sediment archive from the Tarfaya-Laayoune Basin, Morocco, *Paleoceanography*, *32*, 923–946, doi:10.1002/2017PA003146.

Received 4 MAY 2017
Accepted 7 AUG 2017
Accepted article online 11 AUG 2017
Published online 31 AUG 2017

1. Introduction

Global $\delta^{13}C$ increases in the marine and terrestrial carbon reservoirs, related to enhanced marine productivity and carbon burial [e.g., *Arthur et al.*, 1988], are associated with the two most intense Cretaceous Oceanic Anoxic Events (OAEs): the Selli Event or OAE1a in the early Aptian (~122 Ma) and the Bonarelli Event or OAE2, in the late Cenomanian (~94 Ma). Numerous stable isotope records across OAE2 in Atlantic and Tethyan pelagic successions, characterized by low to intermediate sedimentation rates, depict the onset of the event as continuous positive 2.5 ‰ (marine carbonate carbon) to 4.5‰ $\delta^{13}C$ (marine organic carbon) shifts, followed by a characteristic double peak of high $\delta^{13}C$ values and a plateau of several 100 kyr duration before $\delta^{13}C$ values return to background levels [e.g., *Tsikos et al.*, 2004]. The environmental boundary conditions and triggering mechanisms leading to the onset of OAEs remain, however, challenging issues.

A massive injection of isotopically depleted carbon, triggering a major disturbance in the terrestrial and marine carbon cycle and ultimately leading to widespread anoxia and/or acidification in the ocean, is a plausible scenario for Cretaceous OAEs, Paleogene and Neogene global ocean warming events [*Larson and Erba*, 1999; *Storey et al.*, 2007; *Holbourn et al.*, 2015]. Distinctive negative carbon isotope excursions that have been related to degassing of ^{13}C depleted volcanogenic CO_2 often precede the main positive carbon isotope shifts in the earliest part of these warming events. Recently, osmium isotope records indicated a synchronous decrease in $^{187}Os/^{186}Os$ at the onset of OAE2, suggesting that volcanic degassing from the Caribbean Large Igneous Province were the source of the unradiogenic osmium [*Turgeon and Ceaser*, 2008; *Du Vivier et al.*, 2014]. However, negative excursions preceding OAE2 have so far not been reported from most of

the OAE2 records [i.e., *Tsikos et al.*, 2004; *Erbacher et al.*, 2005], except in records from shallow shelf sections in Wunstorf, northern Germany [*Voigt et al.*, 2008], and Oued Mellegue, Tunisia, [*Nederbragt and Fiorentino*, 1999], where sharp negative spikes were recorded at the base of the OAE2 carbon isotope excursion. In southern Mexico [*Elrick et al.*, 2009], a combined stratigraphic and $\delta^{13}C$ study of expanded platform carbonates revealed that the main positive shift was preceded by two extended negative excursions, showing similarities to the negative excursions at the onset of OAE1a in expanded sections of shelf carbonates within the Provence platform [*Lorenzen et al.*, 2013]. However, evidence for negative carbon isotope excursions preceding the characteristic global $\delta^{13}C$ increases associated with the main Cretaceous OAEs remains ambiguous, partly due to incomplete or condensed marine sedimentary records in the earliest stage of OAEs. One possibility is that the absence or spiky character of negative carbon isotope excursions at the onset of OAE2 in deep water sections may be caused by the presence of hiatuses or by condensed sedimentation, related to a sea level maximum within this interval. Furthermore, the conventional sampling resolutions for "high-resolution" stable isotope records, ranging between 10 cm and 1 m, may be insufficient to resolve negative excursions in laminated sediments, characterized by extremely low sedimentation rates.

Organic and carbonate carbon isotope values across OAE2 exhibit two main characteristics: (1) marine organic $\delta^{13}C_{org}$ was significantly lighter (-24 to -28‰ versus VPDB) than in equivalent Miocene to modern organic carbon rich strata (-16 to -23‰)[*Dean et al.*, 1986] and (2) in contrast, bulk marine $\delta^{13}C_{carbonate}$, which, today, is approximately in equilibrium with near-surface dissolved inorganic carbon (DIC) of -1 to 1‰, was considerably heavier during the Cenomanian–Turonian (in the range of 2 to 4.5‰). A long-held view is that higher pCO_2 levels may explain lighter marine $\delta^{13}C_{org}$ values in Earth's climate history [*Hayes et al.*, 1999; *Dean et al.*, 1986] and that changes in marine $\delta^{13}C_{org}$, when normalized against the $\delta^{13}C$ of contemporary DIC or bulk carbonate $\delta^{13}C_{carbonate}$, may be an indicator of changes in pCO_2 levels [*Kump and Arthur*, 1999; *Jarvis et al.*, 2011]. In particular, the main positive $\delta^{13}C$ shift at the onset of OAE2 (~4‰ in $\delta^{13}C_{org}$ versus only 2.5‰ in $\delta^{13}C_{carbonate}$) would correspond to a major pCO_2 reduction and reflect a significant drawdown of atmospheric CO_2 [*Barclay et al.*, 2010]. The relationship between $\Delta\delta^{13}C_{carbonate\text{-}organic}$ and atmospheric pCO_2 levels has been recently used to explain a distinct cooling event, which immediately follows the initial $\delta^{13}C$ shift at the onset of OAE2, the so-called "Plenus Cold Event" [*Gale and Christensen*, 1996; *Jarvis et al.*, 2011; *Jenkyns et al.*, 2017].

Bulk and organic $\delta^{13}C$ curves spanning OAE2 were previously generated in expanded sedimentary successions from outcrop sections and exploration wells S13, S57, and S75 in the Tarfaya Atlantic Margin Basin, Southern Morocco [*Kuhnt et al.*, 1990, 1997; *Tsikos et al.*, 2004; *Kuhnt et al.*, 2005; *Aquit et al.*, 2013]. Previous studies of orbital cyclicity and biostratigraphy in cored exploration wells revealed that the obliquity signal of the Milankovitch frequency band is most prominent in the record of organic matter and carbonate accumulation across the Cenomanian-Turonian boundary [*Kuhnt et al.*, 1997; *Meyers et al.*, 2012a]. These studies, in combination with stable isotope and organic matter accumulation records [*Kuhnt et al.*, 1990, 2005; *Tsikos et al.*, 2004; *Kolonic et al.*, 2002, 2005; *Schönfeld et al.*, 2015], also showed that the Tarfaya Basin has potential for high-resolution supraregional stratigraphic correlation of carbon and oxygen isotope records. Moreover, fluctuations of intermediate water oxygenation during the OAE2 were intially correlated to a Milankovitch framework and the duration of these events assessed on millennial time scales [*Kuhnt et al.*, 1997, 2005; *Meyers et al.*, 2012a]. However, these earlier studies of orbital cyclicity during OAE2 in the Tarfaya Basin mainly used relatively low-resolution wireline logging data and/or focused on the main $\delta^{13}C$ increase, plateau, and recovery rather than on the onset of OAE2. Since these older commercial wells were targeted for black shale exploration, the recovered cores were not suitable for continuous high-resolution sediment logging and the cored material did not fully recover the onset of OAE2 below the organic carbon-rich zone.

To address these shortcomings, a new complete sediment record of OAE2 was recently drilled in the most distal and expanded part of the Tarfaya Basin in southern Morocco (Core SN°4). A detailed description and stratigraphic analysis of the upper Albian to Turonian sedimentary succession in Core SN°4 are provided in a separate study. Here we focus on the late Cenomanian interval (98 to 115 m), which allows unprecedented insights into sedimentation patterns, environmental, and geochemical changes prior to and during the early onset of OAE2. Specifically, we present high-resolution isotopic and elemental data that contribute to a better understanding of the temporal relationship and feedback mechanisms between CO_2 exhalation, climate evolution, and the response of the carbon and nutrient cycle during the onset and development of OAE2.

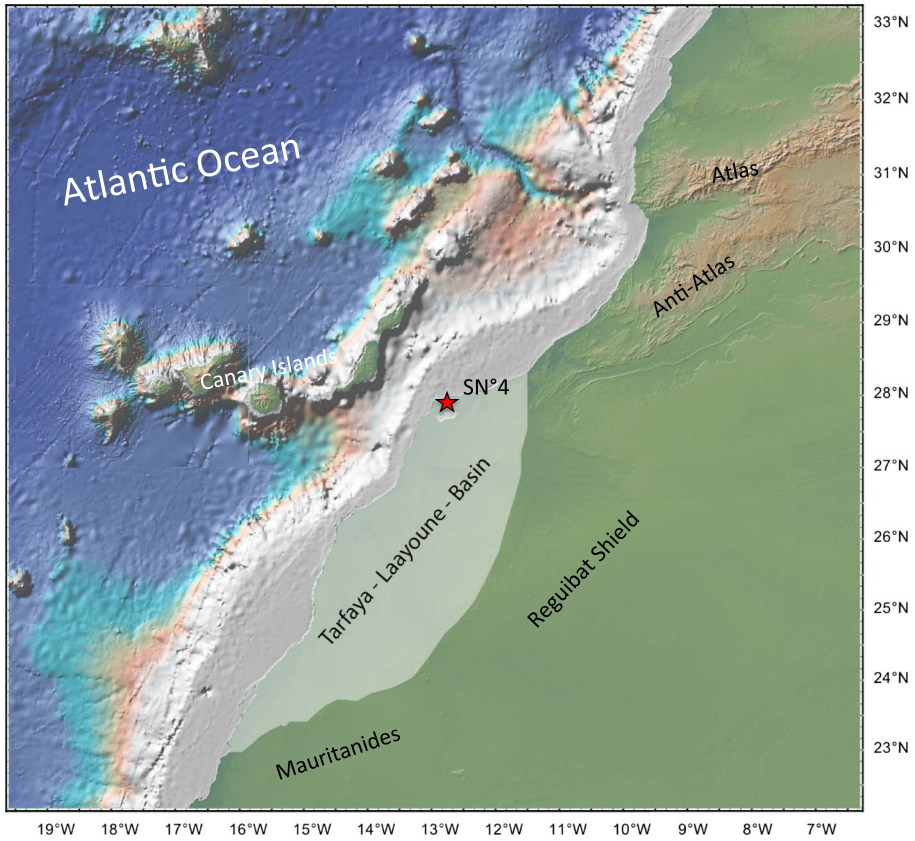

Figure 1. Location of Core in Tarfaya Basin. Map was generated with GeoMapApp (http://www.geomapapp.org), using topography and bathymetry from Global Multi-Resolution Topography synthesis [*Ryan et al.*, 2009].

2. Tarfaya Basin

The Tarfaya Basin extends along the west coast of Africa at latitudes 29 to 22°N and is bounded by the Anti-Atlas mountain chain in the northeast, the Reguibat shield in the east, the Mauritanide chain in the south, and the Atlantic Ocean in the west (Figure 1). The post-Triassic extensional structures and subsidence of the basin are related to the opening of the Atlantic Ocean [*Ranke et al.*, 1982; *Wiedmann et al.*, 1978, 1982; *El Khatib et al.*, 1995, 1996]. Distinctive sedimentary successions are Lower Cretaceous clastic deposits of deltaic or fluvial origin (TanTan Formation) and Upper Cretaceous organic-rich pelagic limestones and marls (Lebtaina Formation [*Ratschiller*, 1970]). Previous paleowater depth estimates for the mid-Cretaceous Tarfaya Basin range between 100 and 300 m [*Kuhnt et al.*, 1986, 2009]. These expanded sedimentary successions were deposited at the northwestern margin of the stable Sahara platform and are unconformably overlain by relatively thin sequences of Cenozoic marginal marine sediments [*Choubert et al.*, 1966].

Approximately 700 m of Upper Cretaceous laminated biogenic sediments, mainly consisting of calcareous nannoplankton, dispersed biogenic silica, planktonic foraminifers, and marine organic matter, were deposited in the Tarfaya Basin, with sedimentation rates exceeding 10 cm/kyr in the depocenter of the basin near the town of Tarfaya [*Leine*, 1986; *Kuhnt et al.*, 1997, 2005; *Kuhnt*, 2001]. These sediments exhibit some of the world's highest accumulation rates of marine organic matter for the Cenomanian and Turonian stages, allowing investigation of paleoceanographic and climate events on a centennial to millennial time scale resolution, comparable to the resolution of Pleistocene paleoclimatic archives.

The estimated areal extent of the Tarfaya Basin ranges from 53,753 km^2 [*Elbatal et al.*, 2010] to 124,821 km^2 (http://www.onhym.com/en/minerals-laboratory/39-en/petroleum/205-tarfaya-lagwira-basin.html) and to as much as 170,000 km^2 [*Leine*, 1986], depending on the definition of its southern margin and consideration of its offshore extent. This huge area and the extremely high accumulation rates of organic carbon during OAE2 indicate that the Tarfaya Basin was an extensive carbon sink at that time, even on a global scale. *Kolonic et al.*

[2005] calculated an annual burial of ~6×10^{10} mols C per year for the Tarfaya Basin during OAE2, which corresponds to ~2% of the overall global excess organic carbon burial in an area equivalent to only ~0.05% of the Cenomanian ocean floor. Major changes in organic carbon accumulation in the Tarfaya Basin and its even larger extension to the South, the Senegal-Casamance offshore basin, thus, likely had direct repercussions on the global carbon cycle and $\delta^{13}C$ budget.

3. Material and Methods

3.1. Tarfaya Core SN°4: High-Resolution Record of OAE 2 Onset

Drill core Tarfaya SN°4 was recovered with the assistance of ONHYM (National Office of Hydrocarbons and Mines of Morocco) in December 2009 close to the main road from TanTan to Tarfaya, ~40 km east of the town of Tarfaya (27°59′46.4″N, 12°32′40.6″W). A total of 350 m of sediment were recovered with a Salzgitter WD3500 hydraulic drilling system. Metal core barrels of 3.05 m length with a diameter of 8.8 cm were used in the upper part of the hole (from 0 to 120 m) and with a diameter of 6.8 cm in the lower part. Drilled sections of ~3.05 m were divided into segments (~80 cm), which were inserted into plastic sleeves and sealed to avoid desiccation, then stored in wooden boxes for transport. The coring scheme of sections and segments for the studied interval (98–115 m) is provided in supporting information Figure S1 and core photographs of each segment are provided in supporting information Figures S2A–S2F. Segments were subsequently split into archive and working halves with a Kaufmann-Titan diamond rock saw. Coring at this site achieved 100% recovery without coring gaps. Detailed lithological description, core logging data, and intermediate-resolution (~40 cm) organic carbon and stable isotope records over the entire Cretaceous succession are provided in a separate study. The positive carbon isotope excursion associated with OAE2 extends between ~60 and 107 m in SN°4. High-resolution XRF scanning (1 cm spacing) and analysis of carbonate, organic carbon, and stable isotopes (2 cm spacing) between 98 and 115 m provide unprecedented resolution over the onset and early development of OAE2 in the Tarfaya Basin.

3.2. Wireline Logging

Wireline logging of Core SN°4 was performed by Geoatlas Laayoune using a Century geophysical well logging system with a natural gamma ray (NGR) sensor. Walls of the hole were not covered with a metal casing and logging depth is recorded relative to the surface with a precision of ±0.1 m. NGR measurements (10 cm spacing) are reported in counts per second (cps) as API (American Petroleum Institute) radioactivity units.

3.3. X-ray Fluorescence (XRF) Core Scanning

Elemental composition of the sediment was analyzed on the working half core surfaces, using a second generation Avaatech X-ray fluorescence core scanner at the Institute of Geosciences, Christian-Albrechts-University in Kiel. The core surface was polished with fine-grained sand paper, cleaned with distilled water and covered with a 4 μm thick Ultralene plastic film to avoid contamination and to protect the detector. Measurements were taken continuously at 1 cm intervals with a downcore slit size of 10 mm over 1 cm^2. Tube voltage settings of 10, 30, and 50 kV were used with sampling times of 10 s. Raw data spectra were transferred into area counts per seconds (Acps) using the iterative least square software (WIN AXIL) from Canberra Eurisys. Results are reported in logarithms of elemental ratios, which are mostly normally distributed and provide the most easily interpretable signals of relative changes in chemical composition downcore and minimize the risk of measurement artifacts from variable signal intensities and matrix effects [*Weltje and Tjallingii*, 2008; *Rothwell and Croudace*, 2015]. Variations in the abundance of the major elements K, Fe, Ti, Si, and Al are used to reconstruct changes in the terrigenous component [*Peterson et al.*, 2000; *Haug et al.*, 2001; *Mulitza et al.*, 2008; *Tisserand et al.*, 2009; *Govin et al.*, 2012]. We normalized these records against Ca, mainly derived from the biogenic carbonate of marine organisms, and expressed the ratio of terrestrial derived elements versus marine carbonate as Log((Al + Ti + Fe + K + Si)/Ca) or Log (Terr/Ca). Additionally, we used Log(Zr/Rb) as an indicator of grain density and size in the terrigenous component due to changes in the proximity of the sediment source and or bottom current intensity which both are commonly associated with sea level changes. The element Zr is almost exclusively found in the heavy mineral zirconium in sediments, while Rb is mainly replacing K in clay minerals. High Log(Zr/Rb) ratios coincide with large grain sizes due to

the high density of zircons, which can only be transported over larger distances by stronger currents together with comparatively large grains of other minerals such as quartz and carbonates.

3.4. Line Scan and RGB Measurements

Line scan measurements (resolution of 143 pixel per 1 cm or 70 μm per pixel) and photographs were acquired on the polished surface of oriented cores with a Jai CV-L107 3 CCD color line scan camera with three sensors of 2048 pixels and dichroic RGB beam splitter prism (RGB channels at 630 nm, 535 nm and 450 nm). Color measurement in L*a*b* units are derived from RGB digital images.

3.5. Stable Isotope Analysis of Bulk Carbonate

A total of 640 samples (2 and 5 cm spacing) were analyzed for stable isotopes of bulk carbonate. Measurements were made with Finnigan MAT 251 and MAT 253 mass spectrometers at the Leibniz Laboratory for Radiometric Dating and Stable Isotope Research at the Christian-Albrechts University in Kiel. The instruments are coupled online to a Carbo-Kiel device for automated CO_2 preparation of carbonate samples. Samples were reacted by individual acid addition. The systems have an accuracy (on the delta scale) of ±0.05‰ for carbon and ±0.08‰ for oxygen isotopes. Results were calibrated using the National Institute Bureau of Standards and Technology (Gaithersburg, Maryland) carbonate isotope standard NBS 20, internal standards, and NBS 19 and are reported as $\delta^{18}O_{carb}$ and $\delta^{13}C_{carb}$ on the Vienna PeeDee belemnite (V-PDB) scale.

3.6. Stable Carbon Isotope Analysis of Organic Matter

Carbon isotope analyses of organic carbon were performed for 340 samples (5 cm resolution) at the GeoZentrum Nordbayern with a Flash EA 2000 elemental analyzer connected online to ThermoFinnigan Delta V Plus mass spectrometer. Approximately 2 g of sediment were ground in an agate mortar and decarbonatized with 10% hydrochloric acid (HCl) until visible reaction stopped. Subsequently, 25% HCl was added for the dissolution of dolomitic material and the sample agitated overnight. After at least 12 h of exposure, samples were five times rinsed with deionized water, decanted, and dried at 40°C. All carbon isotope values are reported in the conventional δ notation in per mil relative to VPDB (Vienna-PDB). Accuracy and reproducibility of the analyses were checked by replicate analyses of laboratory standards calibrated to international standards U.S. Geological Survey 40 and 41. Reproducibility was ±0.04‰ (1σ).

3.7. Micropaleontology

Micropaleontological samples from bituminous marls with high organic matter content were crushed and processed using an alcoholic solution of anionic tensides (REWOQUAT by REWO-Chemie, Steinau, Germany), which helped to break down indurated samples. Around 50 g of dry sediment from each sample was washed over a 63 μm sieve, dried below 40°C, and then sieved into 63–150, 150–250, and 250–630 μm fractions. Planktonic foraminifers from the 250–630 μm fraction were picked and the main biostratigraphic datums within this interval (extinction of *Rotalipora greenhornensis* and extinction of *Rotalipora cushmani*) were identified at a sample resolution of ~10 cm.

3.8. Determination of Total Organic Carbon (TOC) and Carbonate

For the measurement of total organic carbon and carbonate, we used a Carlo Erba elemental analyzer, which analyzes total carbon, nitrogen, and sulfur in solid samples. The analytical method is based on the complete and instantaneous oxidation of the sample by "flash combustion," which converts all organic and inorganic substances into combustion products. The resulting combustion gases pass through a reduction furnace and are swept into the chromatographic column by a carrier gas (helium). The gases are separated in the column and detected by a thermal conductivity detector (TCD), which gives an output signal proportional to the concentration of the individual components of the mixture. Freeze dried samples were ground in an agate mortar and depending on the carbon concentration, 3 to 20 mg of sediment were weighed into a tin cup for TOC measurement. Organic carbon was determined after removing carbonate carbon by acidification with 0.25 N hydrochloric acid. For each set of samples (n = 50) standards and blanks were measured. Each sample was run as a duplicate, and for long-term precision calculation an internal standard was measured in each set.

4. Results

4.1. Lithology

Most of the upper Cenomanian to lower Turonian organic-rich marlstones in Core SN°4 are laminated, indicating that environmental conditions in the Tarfaya Basin fulfilled the following essential requirements for lamination [*Kemp*, 1996]: (1) short-term variability in sediment supply and physical or chemical conditions resulting in compositional changes and (2) unusual environmental conditions to preserve the laminated sediment fabric from bioturbational mixing. In the Tarfaya Basin, strongly dysoxic to anoxic conditions prevailed at the seafloor and apparent bioturbational mixing is restricted to distinct horizons in the late Cenomanian (Figures 2a–2c). However, the nature of the variability that produced compositional changes in the laminated sediments remains somewhat enigmatic. Visible lamination mainly corresponds to thin light, carbonate-rich layers, largely composed of planktonic foraminiferal tests, and dark organic-rich layers, consisting of kerogen, fine-grained carbonate (coccoliths) with clay minerals as a minor component. The fabric of individual laminae is commonly irregular, lense-shaped, and erosional contacts and even rip-up clasts are common. These features indicate active sediment redistribution by bottom currents and/or internal waves or climatic (storm) events [*Kuroda et al.*, 2005], resembling sea floor conditions in some modern upwelling zones [e.g., Peruvian upwelling, *Schönfeld et al.*, 2015, *Erdem et al.*, 2016].

The interval corresponding to the onset of OAE2 in Core SN°4 is characterized by high lithological variability, ranging from dark brown laminated carbonate-rich marlstones to homogenous or bioturbated light brown limestones (Figures 2a–2c). The size and shape of bioturbation traces point to near sediment surface grazing by a burrowing macrofauna such as gastropods, starfish, and crabs, for which oxygen is a strongly limiting factor to deeply penetrate the oxygen minimum zone in modern upwelling systems [*Mosch et al.*, 2012]. Upper Cenomanian sediments below the onset of OAE2 (115–107 m) commonly exhibit sedimentary features indicating submarine current activity, including ripple laminations, flaser lamination, and irregular erosive contacts (Figure 2a). The initial onset of OAE2 (107–105 m) is composed of laminated dark organic-rich marls, which grade into a distinct homogenous limestone layer, marking the middle of the initial positive OAE2 carbon isotope shift at ~105 m core depth. This limestone bed is clearly bioturbated at the top, indicating condensed sedimentation, and the bed is overlain by brownish marlstones with intense bioturbation (Figure 2b). This bioturbated interval is finally capped by laminated marlstones (103.97–104.33 m) with distinct millimeter-scale dark organic-rich and light carbonate-rich layers (Figure 2b). However, the thickness of laminae is very irregular and they are often laterally discontinuous, suggesting that they may result from winnowing by submarine currents rather than represent varved sediments of seasonally or interannually changing biogenic or terrigenous fluxes. The upper part of the studied succession (97.8 to 103.97 m) consists mainly of dark, laminated marlstones with only few intervals of lighter, more calcareous intercalations, which still have preserved lamination (Figure 2c).

4.2. Chronology

The chronology is based on the cyclostratigraphic framework of *Meyers et al.* [2012a], which was developed using evolutive harmonic analysis of the bed resolution density log of well Tarfaya S13 [*Leine*, 1986; *Kuhnt et al.*, 1997] with the following astronomical target periodicities from *Laskar et al.* [2011]: 405 kyr, 127 kyr, and 97 kyr for eccentricity, 49 kyr and 38 kyr for obliquity and 22 kyr and 18 kyr for precession [*Meyers et al.*, 2012a; *Ma et al.*, 2014]. In the interval between cycles −2 and cycle 3, all target periodicities are represented in the Tarfaya sediment record with a probability of 90% or more [*Meyers et al.*, 2012a]. We derived the age model for Core SN°4 by tuning the gamma ray log to the bed resolution density record of well S13 [*Meyers et al.*, 2012a] using 21 tie points (Figure 3). We adjusted the Cenomanian/Turonian boundary (top of cycle 3 with the first occurrence of the calcareous nannoplankton species *Quadrum gartneri* [*Tsikos et al.*, 2004] to the new Ar/Ar age of the C/T boundary in the Western Interior Basin of 93.90 Ma [*Meyers et al.*, 2012b]) (Figure 4). Sedimentation rates generally range between 4 and 9 cm/kyr with a mean of 7 cm/kyr from 93.2 to 94.6 Ma. Sedimentation rates decrease to 4–7 cm/kyr during the onset of OAE2 (94.4 to 93.9 Ma) and increase to 7–9 cm/kyr at the Cenomanian/Turonian boundary (93.9 Ma). In a recent study of the cyclostratigraphy of Cretaceous OAEs, based on the sedimentary record of the Umbrian Apennines, the onset of OAE2 was tuned to a 405 kyr eccentricity maximum [*Batenburg et al.*, 2016]. This interval of increased variability in seasonality follows a prolonged period of low seasonal extremes associated with a 2.4 Myr eccentricity minimum. Following this approach, *Batenburg et al.* [2016] came to the conclusion that the

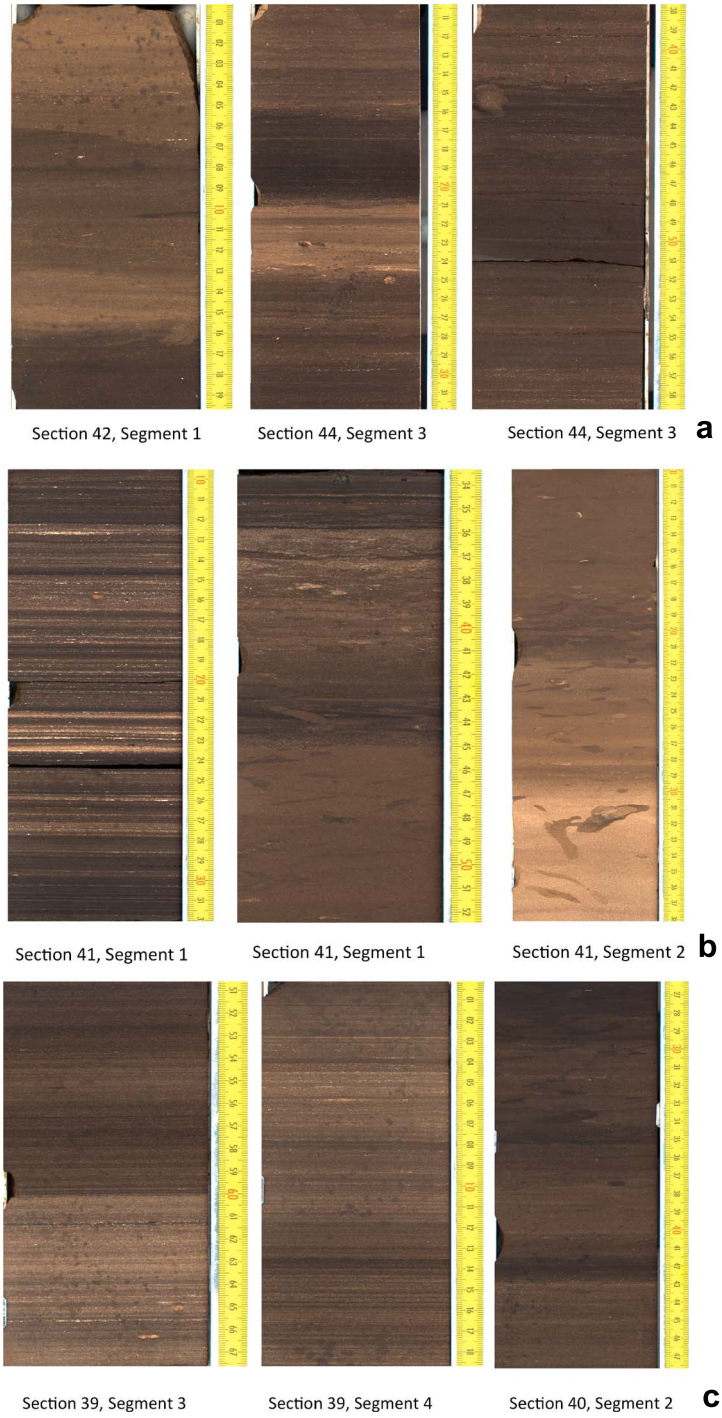

Figure 2. (a) Typical sediment types prior to onset of OAE2 in Core SN°4. Irregular erosive contacts indicating current activity at ocean floor (Section 42, Segment 1, 0–20 cm). Ripple lamination (Section 44, Segment 3, 20–22 cm), and irregular flaser laminated intervals (Section 44, Segment 3, 38–43 cm) indicate active bottom currents. (b) Typical sediment during onset of OAE2 in Core SN°4. Dark and light laminated marlstones with irregular thicknesses of laminae (Section 41, Segment 1, 10–32 cm). Flaser-laminated strongly bioturbated sediments (Section 41, Segment 1, 34–52 cm). Note that dark interval at 43–44 cm is characterized by unusually high P content (81.3 ppm) and low C/P ratio (1.8), indicating unusual enrichment of nutrients. Last occurrence of *R. greenhornensis* occurs at 41–43 cm, whereas sample at 31–32 cm only contains *R. cushmani* and sample residue mainly consists of phosphatic fish debris. Transition of homogenous limestone to bioturbated dark gray marlstone, corresponding to transgressive surface (TS) at ~105 m (Section 41, Segment 2, 30 cm). (c) Typical sediment during early development of OAE2 in Core SN°4. Dark and light laminated marlstones with irregular thicknesses of laminae. (Section 39, Segments 3 and 4). Flaser-laminated strongly bioturbated sediments (Section 40, Segment 2).

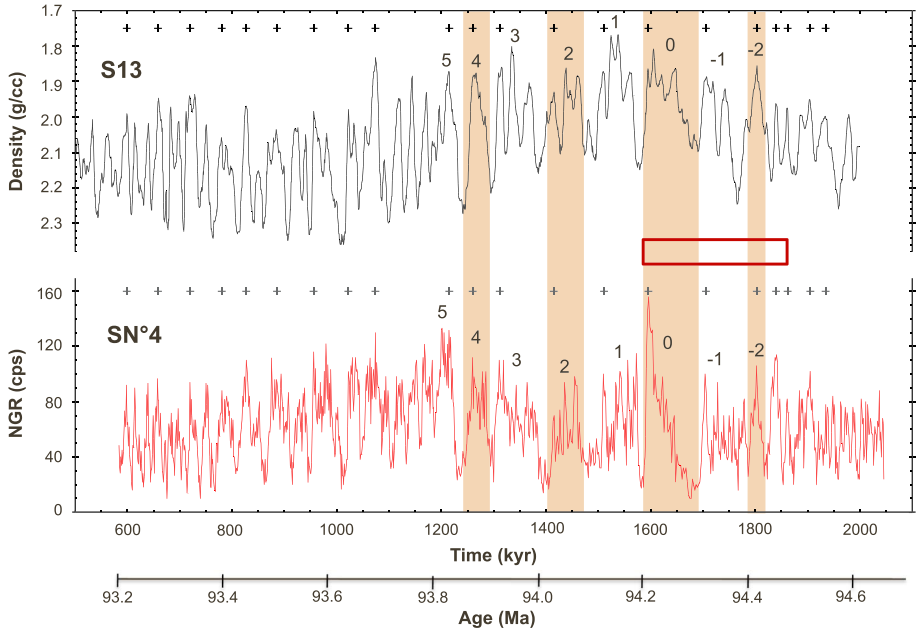

Figure 3. Correlation of Core SN°4 natural gamma ray log (NGR) to density log of Shell/ONAREP well S13 [*Kuhnt et al.*, 1997] using age model of *Meyers et al.* [2012a, 2012b]. Age correlation tie points are marked by crosses. Numbers of cycles −2 to 5 refer to the numbering scheme of *Kuhnt et al.* [1997]. Red box indicates onset and development of OAE2.

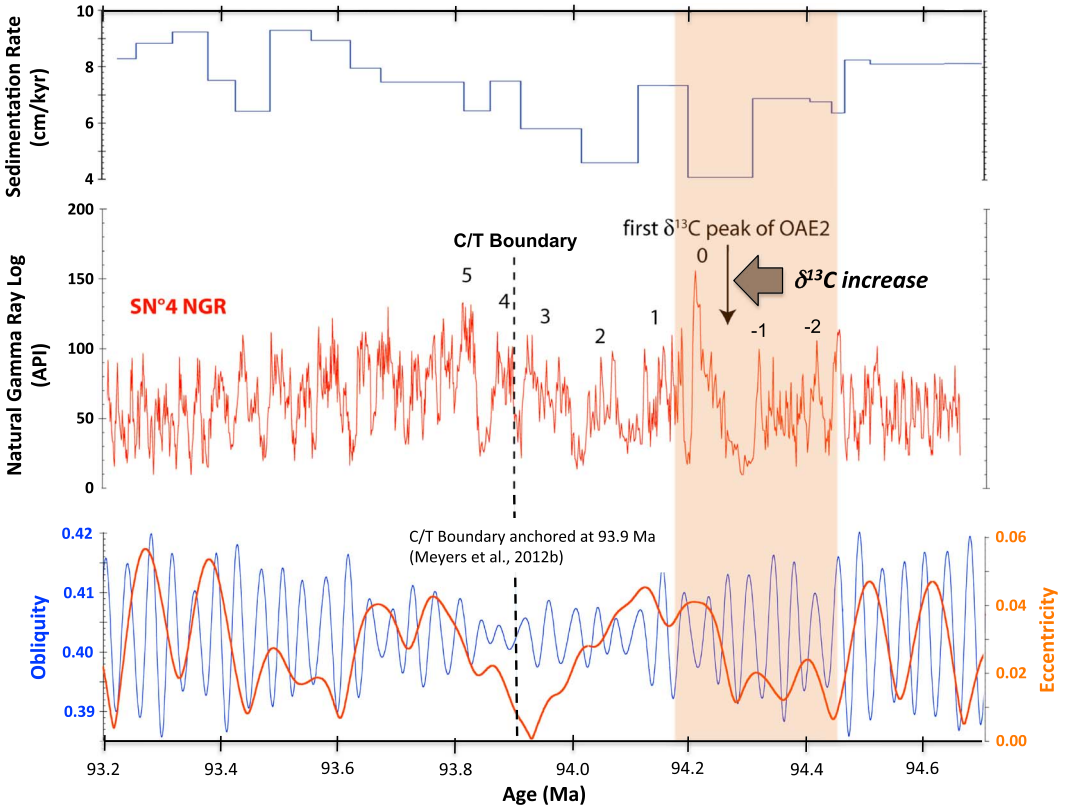

Figure 4. Sedimentation rates and NGR cycles in Core SN°4 following orbitally tuned age model of *Meyers et al.* [2012a] and orbital solution of *Laskar et al.* [2004]. Numbers of cycles −2 to 5 refer to the numbering scheme of *Kuhnt et al.* [1997]. Orange shading marks onset and early development of OAE2.

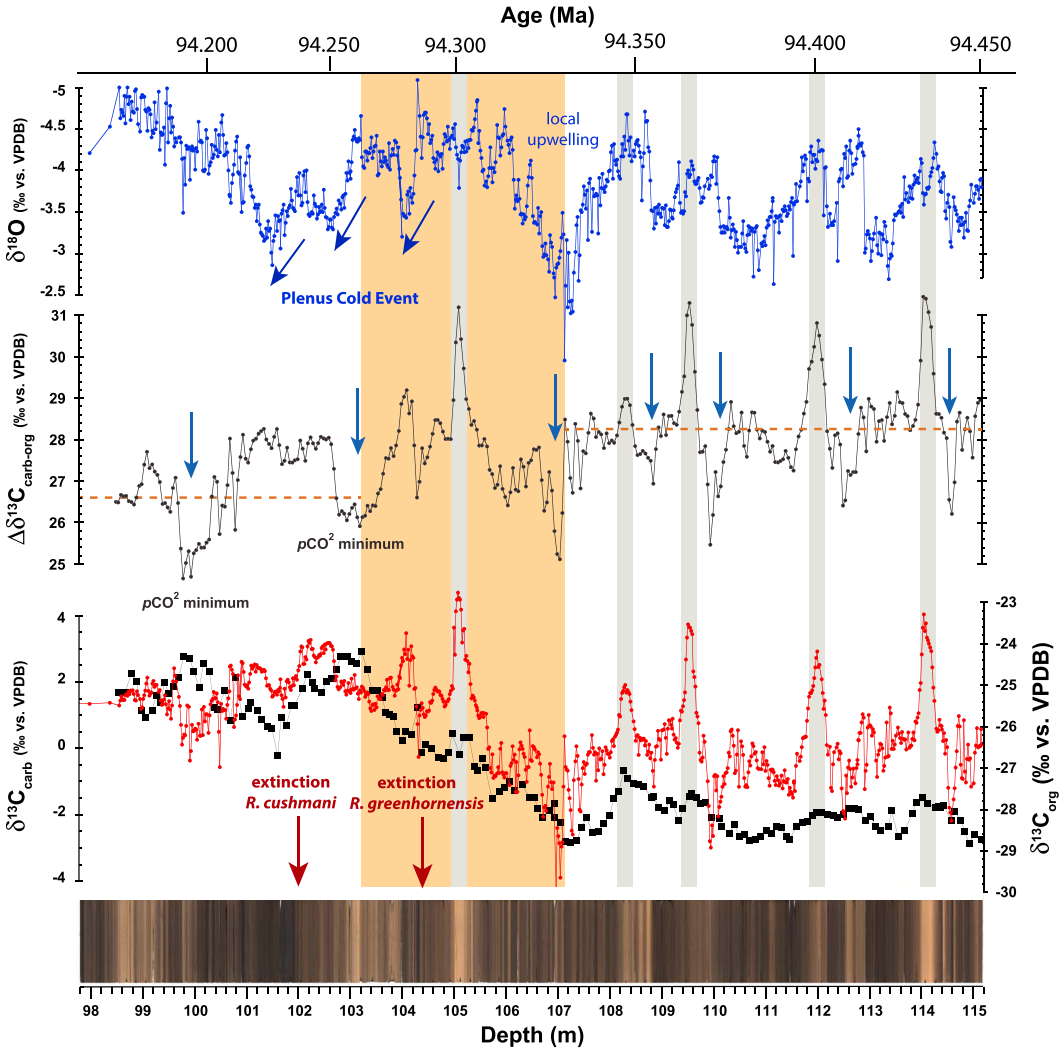

Figure 5. Line scan photographs and high-resolution organic carbon and bulk carbonate carbon isotope records ($\delta^{13}C_{org}$ and $\delta^{13}C_{carb}$) spanning the onset and development of OAE2 in Core SN°4. Orange shading marks main $\delta^{13}C_{org}$ increase, which defines onset of OAE2. Gray shading highlights local maxima in $\delta^{13}C_{carb}$ related to periodic breakdowns of Tarfaya upwelling system. $\Delta\delta^{13}C_{(carb\text{-}org)}$ is strongly driven by diagenetically enhanced high variability in $\delta^{13}C_{carb}$ but reflects in its general trend global decrease of $\Delta\delta^{13}C_{(carb\text{-}org)}$ during main positive carbon isotope excursion and ensuing atmospheric pCO_2 minima and cooling events (Plenus Cold Event). Brown dashed lines indicate average $\Delta\delta^{13}C_{(carb\text{-}org)}$ before (~28.2‰) and after (~26.6‰) main $\delta^{13}C_{org}$ increase (carbon burial event). Blue arrows mark pCO_2 minima, apparently paced by orbital obliquity.

eccentricity maximum at 94.17 ± 0.15 Ma is the likely candidate for an orbital trigger of OAE2, although they could not exclude the preceding eccentricity maximum at ~94.57 Ma as a possible timing for the onset of OAE2, which would be in agreement with our tuning approach.

4.3. High-Resolution Carbonate and Organic Carbon Isotope Records of OAE2

4.3.1. High Variability in $\delta^{13}C_{carb}$

The late Cenomanian $\delta^{13}C_{carb}$ record in Core SN°4 is characterized by five sharp positive excursions, centered at 114, 112, 109.5, 108.3, and 105 m. Except for the excursion at 109.5 m, these excursions coincide with intervals of light, homogenous, or bioturbated sediments with high carbonate content and low TOC (Figure 5), indicating relatively well-oxygenated bottom water conditions and reduced primary productivity. The $\delta^{13}C_{carb}$ peaks at 114, 108.3, and 109.5 m are also represented in the $\delta^{13}C_{org}$ record, indicating short-lived positive excursions preceding the main $\delta^{13}C$ increase of OAE2. In particular the $\delta^{13}C_{carb}$

peak centered at 109.5 m, which coincides with the first $\delta^{13}C_{org}$ increase, is not related to a major change toward carbonate-rich lithology and, thus, appears unaffected by changes in carbonate components or early diagenetic cementation. The reoccurrence of these $\delta^{13}C_{carb}$ peaks and their spacing at ~2 m intervals with sedimentation rates between 7 and 4 cm/kyr suggest that the pacing of these events is controlled by orbital obliquity. The last and most intense of these events (at 105 m) occurs in the middle of the main $\delta^{13}C_{carb}$ shift from long-term averages of −0.5 to +2‰ between 107 and 104 m, which coincides with the $\delta^{13}C_{org}$ shift from −28.5 to −24.5‰.

4.3.2. Negative Carbon Isotope Excursions Prior to the Onset of OAE2

A remarkable feature of the SN°4 $\delta^{13}C$ record is a pronounced negative excursion in $\delta^{13}C_{carb}$ (minimum of ~−4‰) and $\delta^{13}C_{org}$ (minimum of −28.9‰) between 107.8 and 106.8 m, which precedes the main positive shift characterizing OAE2 (Figure 5). This interval consists mainly of dark, commonly laminated marlstones with intermediate TOC values between 5 and 10%, as in underlying upper Cenomanian organic-rich intervals. In addition, $\delta^{18}O$ values are unusually high, which may indicate enhanced local upwelling of relatively cool, saline water masses. This negative $\delta^{13}C$ trough was preceded by an initial increase in $\delta^{13}C_{org}$ with a peak in both $\delta^{13}C_{org}$ (~−27 ‰) and $\delta^{13}C_{carb}$ (~2‰) centered at 108.3 m, which was associated with a decrease in bulk $\delta^{18}O$ values.

4.3.3. Punctuated Main $\delta^{13}C$ Increase

The main positive shift in $\delta^{13}C_{org}$ from 28.5 to 24.5‰, which defines the onset of OAE2, occurs between 107 and 103 m in Core SN°4 (Figure 5). The duration of this main shift can be calculated as ~80–100 kyr (4 m sediment thickness at sedimentation rates of 4–5 cm/kyr), which corresponds to the duration of two obliquity or one short eccentricity cycle. Moreover, the main $\delta^{13}C$ increase was punctuated, close to its midpoint (105 m), by a plateau in organic $\delta^{13}C_{org}$ and a distinct peak in bulk carbonate $\delta^{13}C_{carb}$. The double peak in $\delta^{13}C_{org}$, characteristic of the early part of OAE2 in the Tarfaya Basin and global record [*Tsikos et al.*, 2004; *Kuhnt et al.*, 2005; *Erbacher et al.*, 2005], occurs at 103 and 100 m in Core SN°4. Within this interval, two $\delta^{13}C_{carb}$ maxima are centered at 102.5 and 101 m. Following these maxima, a plateau in both $\delta^{13}C_{carb}$ (fluctuating between ~1.5 and 2‰) and $\delta^{13}C_{org}$ (~ − 25‰) begins above 100 m.

4.3.4. Decrease in $\Delta\delta^{13}C_{(carb\text{-}org)}$ During the Carbon Isotope Shift at the Onset of OAE2

The difference between $\delta^{13}C_{carb}$ and $\delta^{13}C_{org}$ ($\Delta\delta^{13}C_{(carb\text{-}org)}$), which has been suggested to be an indicator of atmospheric/upper ocean pCO_2 concentrations [*Jarvis et al.*, 2011, 2015], is overall lower after the main positive carbon isotope shift (mean of 27.43‰ between 98.5 and 103 m) than before (mean of 28.24‰ between 107 and 115.2 m) (Figure 5). It reaches an overall minimum at ~100 m, following the peak Plenus Cold Event and the extinction of *R. cushmani*. This general pattern is in accordance with previous observations [*Jarvis et al.*, 2011] that $\Delta\delta^{13}C_{(carb\text{-}org)}$ and atmospheric pCO_2 decreased during the Plenus Cold Event. Moreover, the evidence for pCO_2 drawdown during the initial parts of the two main OAE2 $\delta^{13}C_{org}$ excursions based on stomatal index [*Barclay et al.*, 2010] closely match the two major drawdowns interpreted from the $\Delta\delta^{13}C_{(carb\text{-}org)}$ record in SN°4 (supporting information Figure S3). However, this overall trend is strongly overprinted by intense fluctuations in $\delta^{13}C_{carb}$ in the Tarfaya record. These fluctuations are probably caused by periodic breakdowns of the local upwelling system, reflected in substantially increased $\delta^{13}C_{carb}$, possibly combined with some early diagenetic effects in the carbonate-rich sediments characterizing these events.

4.4. $\delta^{18}O$ Fluctuations During OAE2

The bulk carbonate $\delta^{18}O$ record spanning the onset and development of OAE2 exhibits an overall decreasing trend, punctuated by transient episodes of elevated $\delta^{18}O$. Peak warmth is reached during the OAE2 $\delta^{13}C$ plateau ($\delta^{18}O$ of ~−5‰ at ~99 m), whereas the lowest $\delta^{18}O$ values prior to the OAE2 onset are in the range of −4 to −4.5‰ (Figure 5). The most prominent, transient $\delta^{18}O$ increase corresponds to the Plenus Cold Event [*Gale and Christensen*, 1996], which follows the first carbon isotope maximum of OAE2. In Core SN°4 the Plenus Cold Event is expressed as a stepwise $\delta^{18}O$ increase, consisting of three consecutive $\delta^{18}O$ maxima at 104, 103, and 101.5 m interrupted by short warming episodes. The highest $\delta^{18}O$ values (>2.5‰) in the upper Cenomanian of Core SN°4, however, occurred just before the main carbon isotope increase at 107 m in the center of the negative carbon isotope excursion preceding the onset of OAE2. The globally recognized Plenus Cold Event, which is stratigraphically located within the trough between the first and the second peak of the global OAE2 $\delta^{13}C_{org}$ record [*Jarvis et al.*, 2011], is clearly identified in the high-resolution SN°4 $\delta^{18}O$ curve. It is developed as a three-stepped increase in $\delta^{18}O$, which has so far not been recognized in other records.

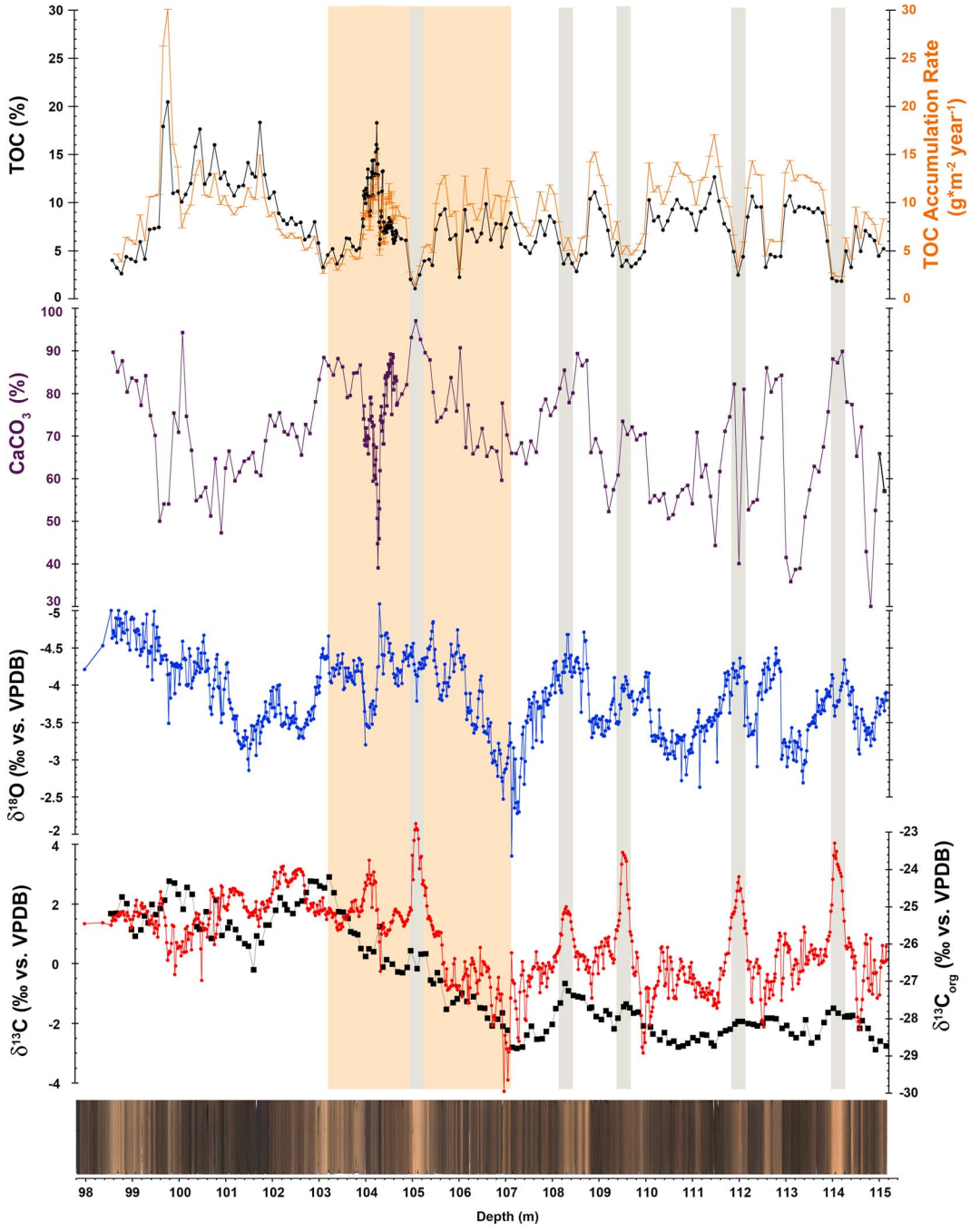

Figure 6. High-resolution $CaCO_3$ and TOC records spanning onset and development of OAE2 in Core SN°4. Line scan and stable isotope records are given for stratigraphic orientation. Orange shading marks interval of $\delta^{13}C_{org}$ main increase, which defines onset of OAE2; gray shading highlights local maxima in $\delta^{13}C_{carb}$.

4.5. Carbonate Content, TOC, and Organic Matter Accumulation Rates

Between 115 and 105 m, TOC values remain relatively low compared to peak OAE2 values, fluctuating around a mean of 6.7% with standard deviation of 2.6%, with a minimum of 1.1% and maximum of 12.7% (Figure 6). In the same interval, the carbonate content exhibits an increasing trend, which is mainly reflected by an increase in the minimum values from just over 30% between 114 and 115 m to 60–70% between 105 and 106 m. Above 105 m, the variability, average, and maximum values in TOC

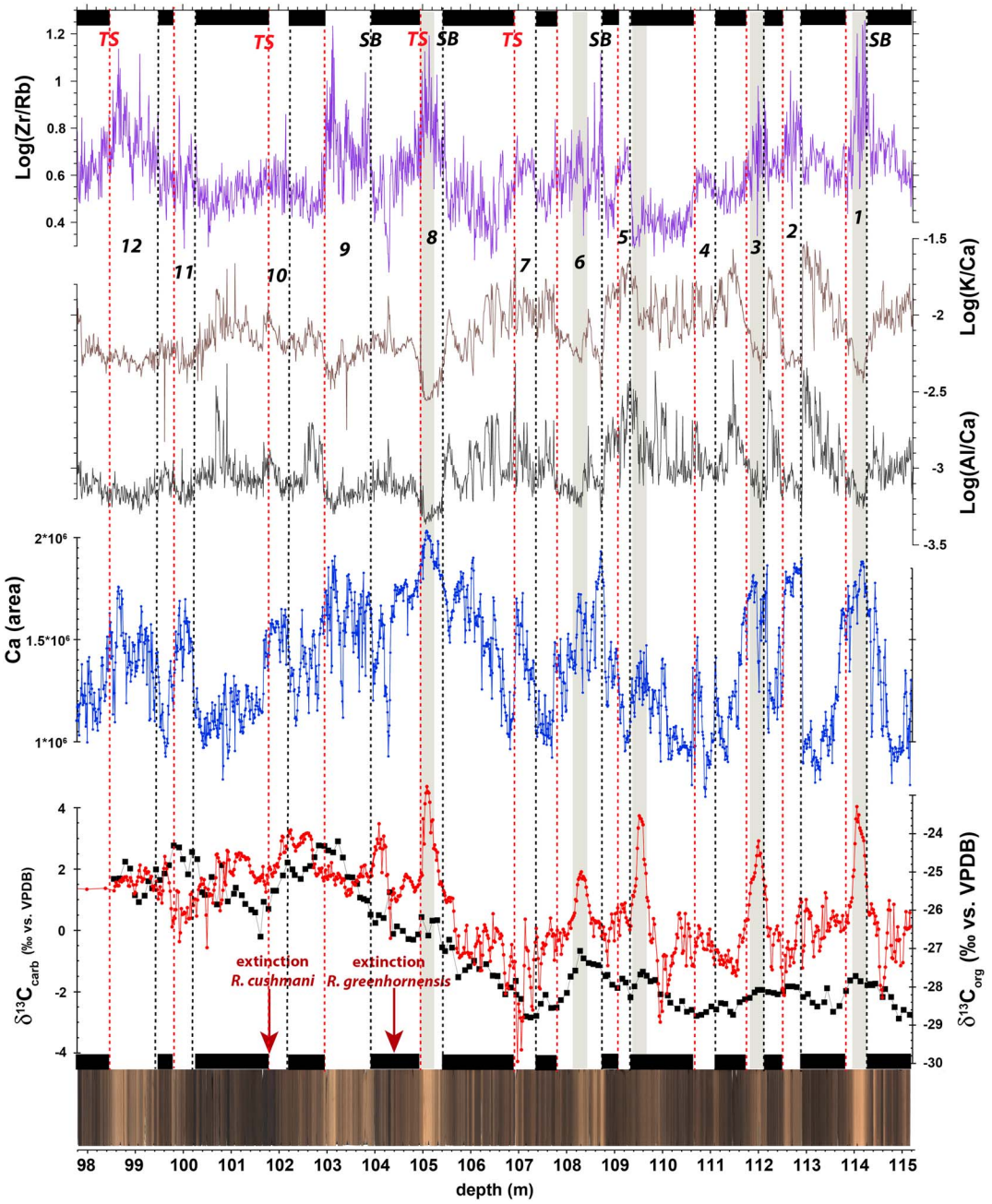

Figure 7. XRF-scanner derived variations in grain density/grains size from Log(Zr/Rb), fine-grained terrigenous flux from Log(Al/Ca) and Log(K/Ca) and carbonate content from Ca area counts (cps) in Core SN°4. Gray shadings indicate $\delta^{13}C_{carbonate}$ maxima; red dashed lines mark changes from carbonate-rich sediments with high Log(Zr/Rb) to carbonate poor sediments with low Log(Zr/Rb), interpreted as transgressive surfaces (TS); black dashed lines indicate changes from organic-rich to carbonate rich sediments associated with increases in Log(Zr/Rb), interpreted as sequence boundaries (SB). Intervals dominated by black laminated organic rich sediments (OMZ expansion and intensification) are marked with horizontal black bars; light, carbonate-rich intervals with elevated Log(Zr/Rb) are numbered from 1 to 12.

increase substantially, reaching a mean of 9.4‰ (3.7% standard deviation) with maximum values of >20% (Figure 6). This stepped increase in TOC variability, average, and maxima parallels the increase in $\delta^{13}C_{org}$ toward the first peak of the OAE2 carbon isotope excursion. However, TOC accumulation rates in the Tarfaya Basin do not exhibit a dramatic increase at the onset of OAE2 and highest accumulation rates are reached after the second $\delta^{13}C$ peak [*Schönfeld et al.*, 2015].

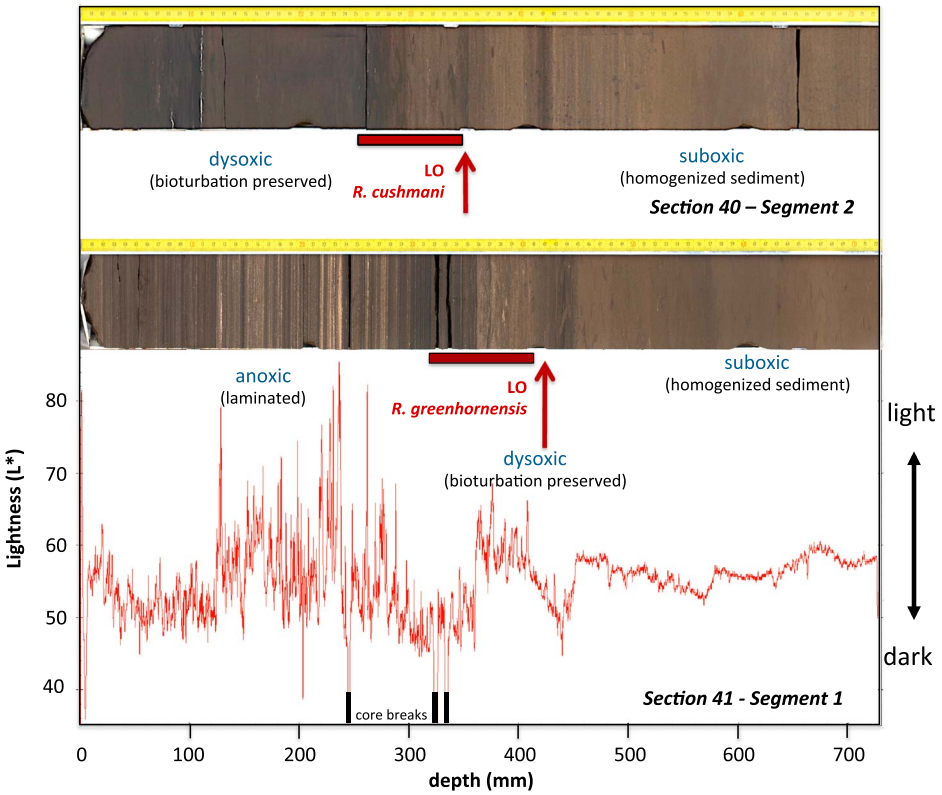

Figure 8. Position of main planktonic foraminiferal extinction events in Core SN°4. Extinction of *R. cushmani* occurs within bioturbated interval and change from light, carbonate-rich suboxic to dark dysoxic conditions. Extinction of *Rotalipora greenhornensis* coincides with onset of laminated sediments, which corresponds in modern upwelling-related OMZs to dissolved oxygen levels below 5 μmol kg^{-1} [*Schönfeld et al.*, 2015]. Red arrows indicate position of last sample with *R. cushmani* or *R. greenhornensis*, red bar marks interval of extinction, between the last sample with and the first sample without *R. cushmani* or *R. greenhornensis*.

4.6. XRF-Scanner Derived Estimates of Terrigenous Supply

Twelve major increases in Log(Zr/Rb) and carbonate can be discriminated in Figure 7. Increases in Log(Zr/Rb) marking increases in grain density and size are associated with coeval decreases in fine-grained terrigenous material (Log(Al/Ca and Log(K/Ca), reflecting abundance of elements mainly bound to clay minerals) (Figure 7). These increases in carbonate grains and coarse terrigenous flux and decreases in clay mineral flux are likely related to falling sea level, shifting the coastline seaward, and promoting resuspension and winnowing transport of fine grained terrigenous material by bottom currents and transport to deeper parts of the basin. The most prominent increases in Log(Zr/Rb) and carbonate occurred at ~114.3, ~108.8, ~105.3, and ~103.9 m. The striking changes from carbonate-rich layers with coarse terrigenous components to black shales with fine-grained terrigenous content, expressed in a subsequent increase of Log(Al/Ca) and Log(K/Ca) at these levels, are interpreted as transgressive surfaces (TS), overlain by laminated organic-rich sediments indicating intensification of upwelling.

4.7. Foraminiferal Extinction Events

The last occurrence of *Rotalipora cushmani* was observed in section 40, segment 2, 34–37 cm (Figure 8) (101.89–101.92 m), which is above the $\delta^{13}C_{carb}$ maximum at 102.0–102.4 m in Core SN°4 and close to the end of the second positive $\delta^{13}C$ shift in the global organic and carbonate $\delta^{13}C$ curves (Figure 7). The extinction interval is bracketed by the sample with the common LO of *R. cushmani* and a sample above in section 40, segment 2, 22–25.5 cm (101.77–101.80 m) that yielded a well preserved foraminiferal assemblage consisting of small hedbergellids. The extinction, thus, occurred close to the peak of the Plenus Cold Event, coincident with the onset of the dark, organic-rich, laminated part of cycle 0 indicating poor bottom water oxygenation (Figure 6).

The LO of *Rotalipora greenhornensis* occurs in section 41, segment 1, 41–43 cm (Figure 8) (104.38–104.40 m) and is bracketed by a sample with common *R. cushmani* and *Whiteinella* spp. in section 41, segment 1, 31–32 cm (104.28–104.29 m), which does not contain *R. greenhornensis* (Figure 8). The extinction interval is, thus, within the lower part of cycle 0 coincident with a distinct decrease in bottom water oxygenation, as shown by a change from light, homogeneous carbonate rich sediments to dark, laminated sediments (Figure 8). The distance between the two extinction events is ~2.5 m or ~40 to 60 kyr considering sedimentation rates of 4–6 cm/kyr in this interval.

5. Discussion

5.1. Fluctuations in Bulk $\delta^{13}C_{carbonate}$: Influence of Global Carbon Reservoir, Carbonate Composition, Local Water Mass Variability and Early Diagenesis

The bulk $\delta^{13}C_{carbonate}$ curve exhibits marked differences to published late Cenomanian bulk $\delta^{13}C_{carbonate}$ records [e.g., *Jarvis et al.*, 2006; *Wendler*, 2013; *Jarvis et al.*, 2015], which show overall higher $\delta^{13}C_{carbonate}$ values and lack the high-amplitude fluctuations, characterizing the late Cenomanian $\delta^{13}C_{carbonate}$ curve in Core SN°4. These high-amplitude fluctuations are reflected by lithological changes and may be easily missing in low-intermediate resolution records as spikes of high $\delta^{13}C_{carbonate}$ generally occur within relatively thin organic carbon-depleted intervals. Peak $\delta^{13}C_{carbonate}$ values remain below 4‰, which is in the normal range of bulk carbonate values in chalk seas that are not affected by upwelling of nutrient-rich intermediate waters. In contrast, lower $\delta^{13}C_{carbonate}$ characterizes laminated organic-rich intervals, when nutrient-rich water masses upwelled to the sea surface. A recent compilation of Late Cretaceous $\delta^{13}C_{carbonate}$ records [*Wendler*, 2013] points to substantial differences (1–2‰) in the amplitude of $\delta^{13}C$ events in the English Chalk reference section [*Jarvis et al.*, 2006], the U.S. Western Interior [*Locklair and Sageman*, 2008; *Sageman et al.*, 2006; *Tessin et al.*, 2015] and eastern Tethys sections in Tibet [*Li et al.*, 2006], which nevertheless all preserve the major features of the global carbon isotope curve. We can exclude the possibility that the composition of bulk carbonate exhibits strong variability across OAE2 in Core SN°4 (Figure 9). In particular, *Pithonella* tests, which occur commonly in more proximal Cenomanian-Turonian limestones in the Tarfaya Basin (i.e., *Kuhnt et al.* [1986], plate 10A) are very rare to absent in the OAE2 interval of Core SN°4. *Pithonella* tests exhibit unusually high carbon isotope values [*Wendler et al.*, 2013], probably related to fractionation during photosynthesis. High proportions of *Pithonella* tests would, thus, explain unusually positive $\delta^{13}C_{carb}$ values in bulk carbonate. A possible influence of vital effects with changing coccolith assemblage composition is unlikely since Cretaceous coccoliths must have used similar carbon acquisition strategies to Paleocene coccolithophorid algae with larger and/or more similar cell sizes and higher atmospheric carbon dioxide concentrations resulting in a smaller range of vital effects than today [*Stoll*, 2005].

Interbasinal and latitudinal differences in the amplitude of Cretaceous $\delta^{13}C$ variations are likely related to locally differing upwelling regimes of nutrient-rich and $\delta^{13}C$-depleted water masses and to the efficiency of the biological pump. Today, in a well-ventilated ocean, the dissolved inorganic carbon of nutrient-rich upwelling water masses can be depleted by >1‰ [*Berger et al.*, 1978]. This may have been substantially higher in the Late Cretaceous Atlantic Ocean, where intermediate water masses were strongly depleted in oxygen and enriched in nutrients and ^{12}C. For example, productivity- and pCO_2-dependent latitudinal differences in the amplitude of the OAE2 carbon isotope excursion (in the range of 1 to 4‰) were recorded in biomarkers for photosynthetic algae [*van Bentum et al.*, 2012]. We consider the generally lower values and high variability on orbital timescales of the $\delta^{13}C$ signal in carbonates from the Tarfaya Basin, which are mainly composed of coccoliths, to be largely a primary signal related to the upwelling of nutrient enriched and $\delta^{13}C$-depleted intermediate water masses. Early diagenesis of organic-rich sediments and preferential formation of ^{12}C enriched authigenic carbonates in organic-rich pore waters may have additionally contributed to high frequency fluctuations in bulk $\delta^{13}C_{carbonate}$ in Core SN°4. In particular, the anomalously low $\delta^{13}C_{carbonate}$ at ~107, ~110, ~112.6, and ~104.5 m may be caused by locally precipitated carbonate cements derived from respired organic matter.

Changes in the global carbon cycle associated with OAE2, i.e., the effect of changing global organic carbon burial rates on the different carbon reservoirs and their isotopic composition, also influence bulk $\delta^{13}C_{carbonate}$. A 2.5% increase in $\delta^{13}C_{carbonate}$, as observed across the onset of OAE2 in Core SN°4, would require burial of ~4500 Gt of organic carbon, assuming that the size of the Cretaceous inorganic carbon

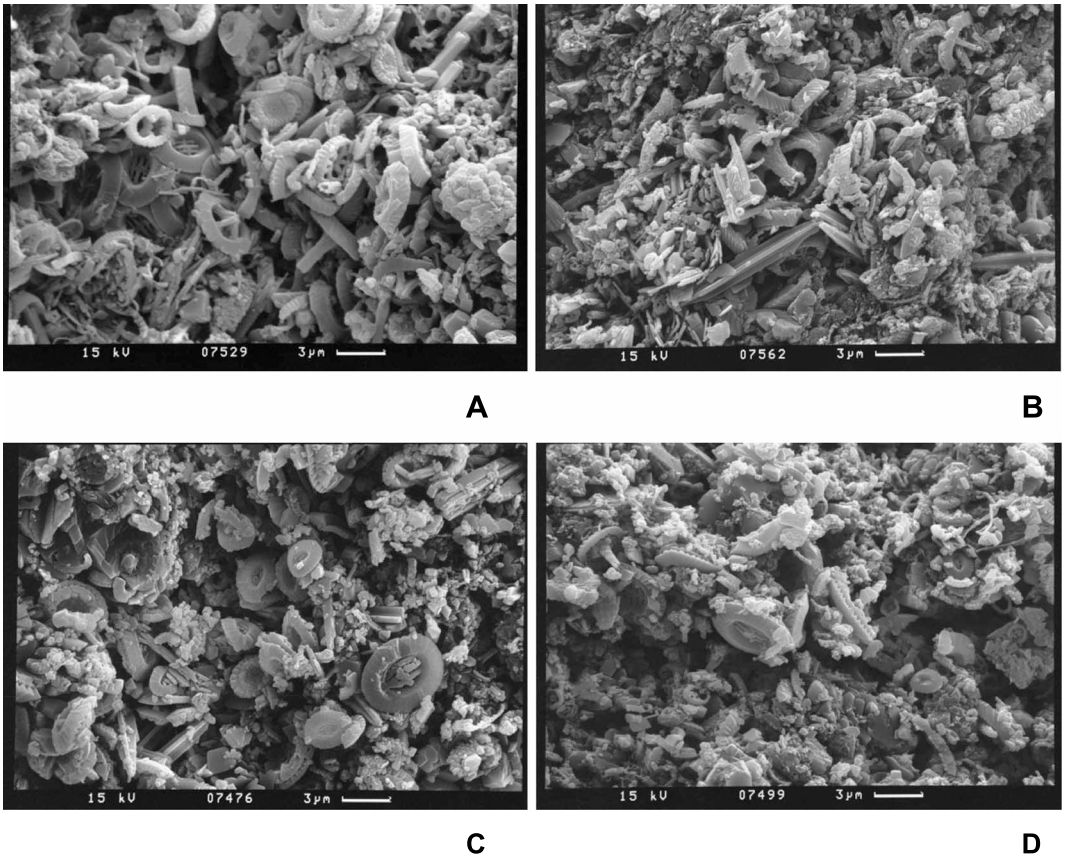

Figure 9. High magnification SEM images of sediment composition in organic-rich laminated and carbonate-rich homogenous intervals with low and high $\delta^{13}C_{carb}$ in Core SN°4. Carbonate fraction is mainly composed of well-preserved coccoliths with no evidence for major diagenetic cementation. (a) Laminated interval: section 41, segment 1, 0–1 cm, 103.80 m. (b) Laminated interval: section 40, segment 4, 0–1 cm, 102.90 m. (c) Light homogenous interval: section 44, segment 2, 40–41 cm, 114.06 m. (d) Light homogenous interval: section 41, segment 2, 43–44 cm, 104.95 m.

pool was similar to today's and $\delta^{13}C_{organic}$ of −25‰ [*Higgins and Schrag*, 2006]. This implies that a 0.1‰ increase in $\delta^{13}C_{carbonate}$ would require a burial of 180 Gt of organic carbon, which is in the range of the modern carbon flux reaching the sedimentary reservoir (100–200 Gt/kyr [*Falkowski et al.*, 1998; *Houghton*, 2007]). To maintain the elevated $\delta^{13}C_{carbonate}$ values during OAE2 over an estimated duration of 500 kyr, a total global excess organic carbon burial of 25,600 Gt would be necessary [*Arthur et al.*, 1988]. This value corresponds to an excess burial rate of 51.2 Gt/kyr or 25–50% of the present-day global organic carbon flux into the sedimentary reservoir. Organic carbon fluxes in the Tarfaya Basin alone, with an extension of ~170,000 km^2 and a burial rate of 10 g/m^{2}*y would amount to 1.7 Gt/kyr or ~1% of the excess burial necessary to produce the positive $\delta^{13}C$ shift at the onset of OAE2 and 3% of the excess burial to maintain the excursion over several 100 kyr. Highly productive subtropical shelf seas were widespread in the Western Tethys during the Cenomanian/Turonian (i.e., Tunisia-Northern Morocco, the huge Senegal Casamance Shelf, and the La Luna Sea in Venezuela), and carbon burial in these seas may have been sufficient to cause and maintain the carbon isotope excursion. However, it remains unclear how the nutrient budgets in these high-productivity areas were balanced over several hundred thousand years.

5.2. Carbon Isotope Fractionation During CO_2 Fixation in Organic Carbon

The $\delta^{13}C$ difference between marine carbonate and the contemporaneously produced organic matter ($\Delta\delta^{13}C_{carbonate\text{-}organic}$) is influenced by two main factors [*Hayes et al.*, 1999]: (1) a temperature dependent fractionation between dissolved inorganic carbon, organic carbon, and carbonate carbon, (2) a fractionation during fixation of CO_2 in organic carbon, which is associated with different algal growth rates and morphologies and correlated to CO_2 concentrations at the sea surface. Likely explanations for the overall lower amplitude of

the $\delta^{13}C_{carbonate}$ excursion at the onset of OAE2, thus, include an overall increase in temperature, especially in the early stage of the OAE, and/or an increase in $\delta^{13}C_{organic}$ fractionation in response to increased algal growth rates and a decrease in pCO_2, in particular during the final stage of the initial shift and ensuing $\delta^{13}C$ plateau.

The $\delta^{13}C_{organic}$ record of bulk organic matter in marine sediments is influenced by various factors, including contamination by terrestrial organic matter, differing rates of local CO_2 uptake in surface waters related to sea surface temperatures and the intensity of upwelling of nutrient-rich water masses and resulting local primary production. In-depth studies of the OM-composition of OAE2 sediments in the Tarfaya Basin showed that any terrestrial contribution, which could result in significant variability in $\delta^{13}C_{organic}$, was negligible [*Kuhnt et al.*, 1990; *Kuypers et al.*, 2002; *Kolonic et al.*, 2005]. However, variable rates of primary productivity may have caused significant spatial and temporal differences in the degree of carbon isotope fractionation, even in marine organic matter [*Laws et al.*, 1995]. Increases in upwelling/productivity promoting phytoplankton growth rates would result in local positive $\delta^{13}C_{organic}$ anomalies and a decrease in $\Delta\delta^{13}C_{carbonate\text{-}organic}$. However, the decrease in $\Delta\delta^{13}C_{carbonate\text{-}organic}$ associated with the Plenus Cold Event appears to be a global phenomenon [*Jarvis et al.*, 2011], probably related to a major drawdown of atmospheric pCO_2.

The variability of intermediate to high-resolution marine organic carbon isotope records at subtropical latitudes is significant. Pre-OAE2 values range from −25 ‰ at the base of the Bonarelli level in central Italy [*Tsikos et al.*, 2004] to −28‰ at Demerara Rise [*Erbacher et al.*, 2005], while values from southern France and the Western Interior Basin [*Jarvis et al.*, 2011; *Du Vivier et al.*, 2015] range between −26 and −27 ‰. The Pre-OAE2 values in Tarfaya SN°4 which vary between −28 and −29 ‰ are thus among the lightest marine late Cenomanian $\delta^{13}C_{organic}$ values, only comparable to ODP Site 367 offshore the Casamance shelf, Senegal [*Kuypers et al.*, 2002]. This geographic pattern of extremely light $\delta^{13}C_{organic}$ values along the tropical Cretaceous West African margin persists through the OAE2 carbon isotope excursion with peak $\delta^{13}C_{organic}$ values around −24‰ in SN°4, in contrast to values around −22‰ at Demerara Rise and between −22 and −23 ‰ at Gubbio and the Western Interior. These geographic differences in $\delta^{13}C_{organic}$ correlate to differences in local productivity [*van Bentum et al.*, 2012] and may be related to intense late Cenomanian equatorial upwelling along the Northwest African continental margin.

An alternative explanation for the relatively light carbon isotopic compositions of organic matter in Tarfaya black shales before, during and after the positive $\delta^{13}C$ excursion associated with OAE2 would be intensified photic zone recycling of isotopically light organic carbon due to intensified surface stratification [*Küspert*, 1982]. Evidence of bacterial nitrogen fixation associated with photic zone anoxia common to OAE2 black shales and Mediterranean sapropels supports such a scenario of intensified surface stratification with enhanced organic carbon oxidation and reutilization in the photic zone [*Meyers et al.*, 2006]. However, even potentially enhanced land-derived nutrient fluxes during times of a greenhouse-amplified hydrologic cycle [*Van Helmond et al.*, 2014; *Meyers*, 2014] do not completely resolve the conundrum of nutrient supply for sustained high organic matter accumulation rates without vertical mixing (upwelling) of nutrient-enriched water masses.

5.3. Impact of Anoxia on the Stepwise Extinction of *Rotalipora greenhornensis* and *Rotalipora cushmani*

The environmental context of the two main global extinction events of keeled planktonic foraminifers (*R. greenhornensis* and *R. cushmani*) in the Tarfaya Basin exhibits striking similarities. Both extinction events occurred during major changes toward poorly oxygenated bottom water conditions (Figure 9) and probably were linked to transient cooling episodes within the Plenus Cold Event (Figures 5, 6). The *R. greenhornesis* extinction occurred during the first step of the three-stepped cooling of the Plenus Cold Event and the *R. cushmani* extinction occurred during the third and main cooling phase of this event.

The stratigraphic position of the two extinction events with respect to the carbon isotope stratigraphy is constrained on a global scale. In a recent study, stepwise marine extinctions across OAE2, including the *R. greenhornensis* and *R. cushmani* extinction events, were correlated to stable carbon isotope curves along a depth transect at the northern Iberian margin [*Kaiho et al.*, 2014]. These authors found the same characteristic extinction pattern at all sections studied, independently of their bathymetric position: (1) the extinction of *R. greenhornensis* was encountered within the center of the main first positive $\delta^{13}C$ shift marking the onset

of OAE2 and the extinction of *R. cushmani* in the trough between the first and second $\delta^{13}C$ maximum of OAE2, ~50 kyr later. A similar relationship between the extinction of the last two rotaliporids and the global $\delta^{13}C$ curve across OAE2 was previously reported from the Western Interior Basin U.S. [*Caron et al.*, 2006; *Desmares et al.*, 2008]; the Eastbourne section, UK [*Paul et al.*, 1999; *Tsikos et al.*, 2004], the Vocontian Basin in southern France [*Grosheny et al.*, 2006; *Desmares et al.*, 2008], Tunisia [*Caron et al.*, 2006], and from outcrop and drill cores in the Tarfaya Basin [*Luderer and Kuhnt*, 1997; *Tsikos et al.*, 2004; *Kuhnt et al.*, 2005]. Thus, we can exclude that the disappearance of *R. greenhornensis* and *R. cushmani* in the SN°4 record was driven by a local expansion of the OMZ and intensification of upwelling. These global extinctions suggest that the expansion of anoxia at 94.24 and 94.29 Ma occurred on a basin-wide scale including the entire Western Tethys and Atlantic/Western Interior Seaway.

Two environmental changes could have affected the habitat space of thermocline dwelling keeled rotaliporids: (1) extreme intensification and expansion of the oxygen minimum zone up to photic zone anoxia, which would have driven the entire habitat of *R. greenhornensis* and *R. cushmani* to become anoxic; and (2) severe ocean acidification within the oxygen minimum zone, which would have affected wall thickness and calcification of these heavily keeled thermocline dwellers [*De Moel et al.*, 2009]. The second mechanism is supported by the fact that both species develop thin walled morphotypes with strongly reduced keels or even completely lost imperforate keels just before their extinction [*Longoria*, 1973; *Luderer and Kuhnt*, 1997; *Desmares et al.*, 2008]. Ocean acidification as a driver of the extinction of rotaliporids during OAE2 is additionally supported by first intermediate resolution Ca-isotope records across the anoxic event from the European Eastbourne and Pont Issole secions and the Portland #1 Core in the U.S. Western Interior Basin [*Du Vivier et al.*, 2015]. Here positive $\delta^{44/40}Ca_{sw}$ excursions, interpreted as changes to the calcium carbonate fractionation factor associated with brief ocean acidification events, precede the $\delta^{13}C$ maxima and thus closely match the *Rotalipora* extinction levels. These environmental deteriorations must have affected the global ocean in order to drive the extinction of these widely distributed tropical-subtropical species. The ~50 kyr offset between the two extinction events (approximating the duration of one obliquity cycle during the Cenomanian) and the almost identical evolution from suboxic to anoxic conditions suggest orbital control on both the spread of ocean anoxia/acidification and the extinction of thermocline dwelling planktonic foraminifers.

5.4. Transient Cooling Events and Sea Level Fluctuations During the Onset of OAE2

Decreasing Log(Al/Ca), Log(K/Ca), and Log(Terr/Ca) and nondissolvable residue, as well as increasing carbonate content, provide clear evidence that terrigenous input decreased in two steps between ~111 and ~105 m, prior to the onset and during the initial phase of OAE2 (Figures 7 and 10). This decrease in terrigenous supply is most likely associated with a shoreward displacement of the shoreline, retraction of river deltas, creation of additional accommodation space on the shelf, and overall reduction of sediment flux to the outer shelf location of Core SN°4 during a major transgressive phase. A first peak transgression (maximum flooding) is reached at ~106 m in the upper part of a thick interval of laminated organic-rich marlstones with minimum Log(Rb/Sr) at the base of the initial $\delta^{13}C_{org}$ increase of OAE2. This transgression has also been documented in the U.S. Western Interior [e.g., *Elder et al.*, 1994; *Arthur and Sageman*, 2004; *Laurin and Sageman*, 2007] and is in broad agreement with the interpretation of the Mexican platform-carbonate sea level record, where the onset of OAE2 is also related to a major transgressive event [*Elrick et al.*, 2009].

A first regressive phase with a distinct sea level lowstand is associated with the very prominent limestone bed centered at 105 m (Figure 7). This regressive phase again matches a similar trend in the Western Interior sea-level record [*Laurin and Sageman*, 2007]. We consider the limestone bed at 105 m as a lowstand deposit between a sequence boundary and a transgressive surface, when the oxygen minimum zone did not impinge on the Tarfaya shelf and the location of Core SN°4 was still well oxygenated. The TS on top of the limestone bed represents the first significant flooding surface at the onset of a new transgressive sequence (sequence Ce5 in the global eustatic cycle scheme of *Gale et al*. [2002]). This TS is typically characterized by a well cemented carbonate surface, which was intensely perforated by burrowing organisms. In shallower shelf areas of the Tarfaya Basin with low sediment supply, where falling sea level and/or lowstand facies are not usually preserved above the sequence boundary due to winnowing by intensified wave induced or tidal currents, hiatuses commonly develop during the sea level lowstands and the TS commonly falls together with the SB. However, in the more distal location of Core SN°4, we consider the relatively coarse grained carbonate beds to represent lowstand deposits, possibly a more distal equivalent of the lowstand skeletal limestones

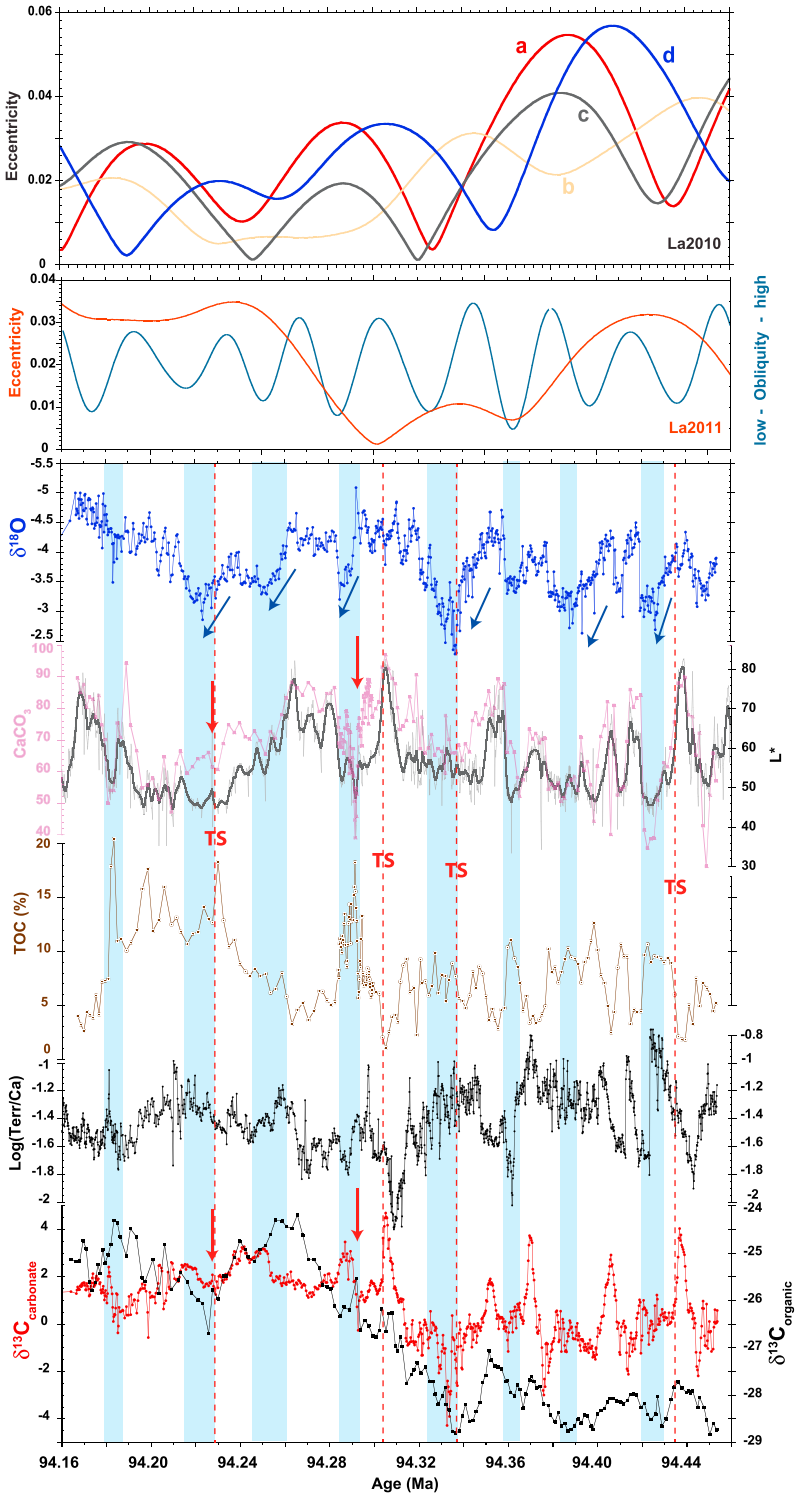

Figure 10. (top and middle) Alternative solutions for orbital eccentricity (La10a-d) from 2011 and for eccentricity and obliquity from 2011. Note that La10a and La10d indicate major decrease in 400 kyr eccentricity culminating in distinct (100 kyr and 400 kyr) eccentricity minimum coinciding with OAE2 onset. (bottom) Core SN°4 proxy records in time domain. Light blue shaded areas indicate "cool" phases, characterized by heavy bulk $\delta^{18}O$, deposition of dark laminated black shales with elevated TOC and clay (Log(Terr/Ca). Major TS (changes from light carbonate rich to dark organic carbon rich sedimentation marked with dashed red lines) coincide with $\delta^{18}O$ minima at obliquity maxima (highest temperature gradients between equator and high latitudes). Red arrows indicate extinction of *R. greenhornensis* and *R. cushmani* at onset of organic-rich laminated sedimentation following TS.

described from the Greenhorn Formation in the Western Interior [*Sageman*, 1996]. Sediments across and immediately overlying the TS are commonly carbonate rich, relatively coarse grained, well oxygenated, and bioturbated. With progressing transgression they grade into organic-rich, laminated, and more fine grained, clay-rich black shales, which are indicative of an impinging oxygen minimum zone on the outer to middle shelf. The interval above the TS (~105–104 m) represents such a typical sea level highstand deposit (Figure 7), whereas a series of progressive stepwise regressions and subsequent transgressions is associated with the Plenus Cold Event. This stepwise cooling culminated at 102–101 m with high $\delta^{18}O$ indicative of cool surface water conditions and organic rich sediments suggesting enhanced upwelling and intensification of the OMZ, which led to the extinction of *Rotalipora cushmani*.

To sum up, the Tarfaya sea level record reveals a long-term (>100 kyr) transgressive cycle before the onset of the main carbon isotope excursion, which reaches its maximum close to the onset of the main positive $\delta^{13}C$ excursion. The following sea level cycle is characterized by a lowstand midway during the positive carbon isotope shift and by a prominent TS at the base of the globally recognized eustatic sequence Ce5, which is correlative to a major hiatus in the more proximal Mohammed Plage Section [*Mort et al.*, 2008; *Kuhnt et al.*, 2009; *Gertsch et al.*, 2010]. The ensuing transgressive trend is punctuated by prominent stepwise regressions including the peak of the Plenus Cold Event coincident with the $\delta^{13}C$ trough between the two $\delta^{13}C$ maxima.

Recently, *Wagreich et al*. [2014], *Sames et al*. [2016], and *Wendler and Wendler* [2016] proposed that net transfer of water to the continent by the infill of dried-out groundwater reservoirs and large inland basins during transitions from arid to humid climate periods may have resulted in significant short-term sea level falls (aquifer eustasy). According to this scenario, rapid eustatic sea level falls (when aquifers and inland basins are filled) are associated with sudden increases in marine $\delta^{18}O$, which would mimic "glaciations" followed by longer periods of warm humid climate with decreasing marine $\delta^{18}O$ and rising sea level. Terrigenous proxies in Core SN°4 indicate a sudden regression during the carbonate maximum centered at 105 m, approximately midway within the initial OAE2 $\delta^{13}C_{org}$ increase and following a prominent decreasing (warming) phase in the long-term $\delta^{18}O$ record, which is in agreement with the aquifer-eustatic scenario. However, the main increase in $\delta^{18}O$ associated with enhanced terrigenous fluxes, indicating closest proximity to land and lowest sea level, occurred gradually (stepwise) starting from 104.5 m to the peak of the Plenus Cold Event between 101 and 102 m. This gradual increase rather supports a glacioeustatic scenario with slow buildup of ephemeral ice caps on Antarctica even under high atmospheric CO_2 conditions [*Flögel et al.*, 2011] rather than rapid infill of continental aquifers.

5.5. Impact of Orbital Forcing on Organic Carbon Burial and Terrigenous Supply

Correlation of the TOC, carbonate, lightness, terrigenous, and stable isotope records in Core SN°4 to the latest orbital solutions encompassing this interval [*Laskar et al.*, 2011] suggests an enhanced response to obliquity forcing during the onset of OAE2. In particular, the punctuation of the main $\delta^{13}C$ increase (approximate duration of 80 kyr) by a plateau in organic $\delta^{13}C_{org}$ and a distinct peak in bulk carbonate $\delta^{13}C_{carb}$ points to obliquity control on carbon isotope variations. Also time series analysis of the logging record from the nearby exploration well S13 [*Meyers et al.*, 2012a] previously indicated a strong sedimentation response to obliquity in the Tarfaya Basin. In contrast, the response to the 100 kyr short eccentricity cycle, considered to be the dominant forcing during periods of greenhouse climate such as the Paleogene warm periods [*Zachos et al.*, 2010; *Kirtland Turner*, 2014], appears muted over this interval (Figures 10 and 11). The onset of OAE2 coincides with an extended interval of low eccentricity, during the low phase of a 400 kyr cycle coincident with dampened variability in short eccentricity and high amplitude variability in obliquity (Figures 10 and 11). This relatively unusual orbital configuration likely accounts for the strong obliquity signal in the proxy records including carbonate content, TOC, lightness, density, and gamma ray data. The same periodicity is also evident in the bulk carbonate $\delta^{13}C$ and, at lower amplitude, in the organic carbon $\delta^{13}C$.

These results suggest that a change from low to high eccentricity at the 400 kyr band, which would result in increased precessional forcing, occurred during the main increase in $\delta^{13}C$ that characterizes the onset of OAE2. A sudden change in orbital cadence from low to high eccentricity could have triggered carbon cycle feedbacks fostering increases in atmospheric pCO_2 in several ways: (1) In analogy to Paleogene "hyperthermal events," rapid warming at high latitudes, related to the onset of precessional insolation maxima, would lead to fast release of greenhouse gases at high latitudes, when Antarctica was largely ice free [*DeConto et al.*,

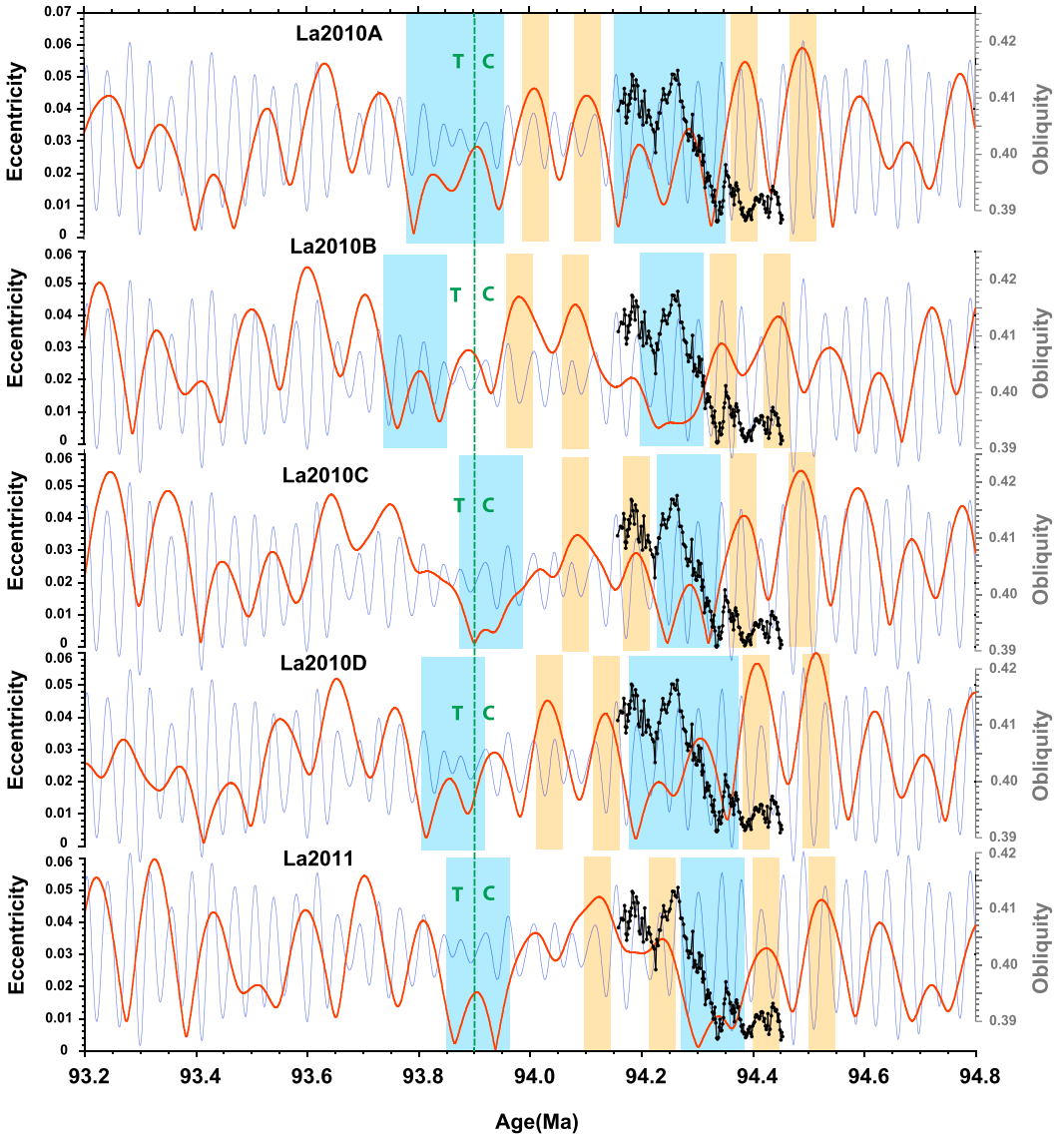

Figure 11. Orbital solutions across OAE2 onset. Orange bands indicate periods of "warm" orbits at 100 kyr eccentricity maxima; blue bands indicate extended periods of cool orbits at 400 kyr eccentricity minima. Even taking into account the relatively wide range of error from alternative orbital solutions, the onset of the positive carbon isotope excursion falls within an extended period of low eccentricity following a ~2 Myr interval of high amplitude 100 kyr eccentricity variability.

2012; *Kirtland Turner*, 2014]; and (2) high-amplitude variability in obliquity additionally result in strong fluctuations in the thermal pole-to-equator gradient, with repercussions on the meridional atmospheric heat and moisture transport and Antarctic climate variability.

On a first view, the strong response of the sedimentary and carbon isotope records to orbital obliquity at low latitudes is puzzling. A previous explanation for obliquity-driven productivity changes along the NW African margin invoked the transfer of high-latitude climate dynamics via fluctuations in the intensity of coastal/equatorial upwelling in combination with changes in the hydrographic properties of the upwelling intermediate water masses [*Kuhnt et al.*, 1997; *Kolonic et al.*, 2005]. However, this model does not explain the strong climate response to obliquity forcing in a greenhouse world on a supraregional scale. Changes in oceanic circulation during OAE 2 represent another likely mechanism for the propagation of a high-latitude signal through latitudinal expansion of a new dense intermediate water mass of high-latitude origin [*Meyers et al.*, 2012a]. A recent study, based on data from temperate Northern Hemisphere sections proposed that the

unusually strong response of the Cretaceous greenhouse climate system to short-term and long-term obliquity forcing was introduced by a transient storage of organic matter or methane in quasi-stable reservoirs including wetlands, soils, marginal zones of marine euxinic strata, and potentially permafrost that responded nonlinearly to obliquity-driven changes in high latitude insolation and/or meridional insolation gradients [*Laurin et al.*, 2015].

An alternative explanation is that orbital obliquity is the primary control on equatorial annual average insolation, which in the modern world has significant impact on West and East Pacific annual average SST and hydroclimate [*Timmermann et al.*, 2007; *Clement and Peterson*, 2008]. The annual mean insolation at the equator fluctuates at the obliquity band by ~3 W/m^2, which translates in numerical models (ECHO-G model [*Timmermann et al.*, 2007]) under modern boundary conditions into obliquity-driven SST changes in the tropical East and West Pacific Ocean that are in the range of 0.7°C. The impact of obliquity-controlled changes in tropical SST on convective and monsoonal precipitation was probably even stronger in the middle Cretaceous water world, which would have had substantial repercussion on tropical weathering and nutrient cycles.

6. Conclusions

The onset of OAE2, which corresponds to a two-stepped increase in $\delta^{13}C_{carbonate}$ and $\delta^{13}C_{org}$ spanning ~100 kyr, is preceded by negative carbon isotope excursions in both $\delta^{13}C_{carbonate}$ and $\delta^{13}C_{org}$ most likely resulting from massive injections of isotopically depleted carbon. During the main $\delta^{13}C$ increase and onset of intense oxygen-depleted conditions, bulk carbonate oxygen and carbon isotopes, terrigenous input, and carbonate and organic matter exhibit a strong response to obliquity forcing. We interpret the top of the carbonate-rich interval, which is virtually devoid of any terrigenous input and characterized by a small plateau in the $\delta^{13}C_{org}$ curve and a distinct short-lived positive $\delta^{13}C_{carb}$ excursion, as the transgressive surface of the latest Cenomanian transgressive cycle.

A three-stepped transient climate cooling (Plenus Cold Event) with intermittent brief warming/anoxia episodes occurred in the latest stage of the main $\delta^{13}C$ increase, reminiscent of the succession of events during OAE-1a [*Kuhnt et al.*, 2011]. We speculate that these cooling events reflect ephemeral Antarctic glaciations, triggered by biological drawdown of atmospheric CO_2 and changes in high latitude radiative forcing at periods of low orbital obliquity and eccentricity. Two major extinction events of thermocline dwelling keeled planktonic foraminifers, *Rotalipora greenhornensis* and *Rotalipora cushmani*, within the Plenus Cold Event appear to be closely linked to obliquity-paced periodic expansions and intensifications of the oxygen minimum zone. Both extinction events were probably associated with development of photic zone anoxia and ocean acidification affecting the habitat space of these species within the upper thermocline.

Acknowledgments
This research was funded by the German Research Council (DFG) in the framework of SFB 754, TP A7. RWE Dea AG in cooperation with the Office National des Hydrocarbures et des Mines, Morocco, enabled drilling SN°4 in the framework of the Atlantic Margin Integrated Basin Analysis Project. We thank Nils Andersen (Leibniz Laboratory for Radiometric Dating and Stable Isotope Research, Kiel) and Michael Joachimski (GeoZentrum Nordbayern, Friedrich-Alexander Universität Erlangen-Nürnberg) for stable isotope measurements, Dieter Garbe-Schönberg and Samuel Müller (Institute of Geosciences, Kiel) for advice with X-ray fluorescence scanning, and Bettina Domeyer (GEOMAR) for technical help with the CHN Analyzer. We gratefully acknowledge constructive reviews from Phil Meyers and Brad Sageman which significantly improved the manuscript. Data will be archived at PANGAEA, data publisher for Earth and Environmental Science, doi:10.1594/PANGAEA.

References

Aquit, M., W. Kuhnt, A. Holbourn, E. H. Chellai, K. Stattegger, O. Kluth, and H. Jabour (2013), Late Cretaceous paleoenvironmental evolution of the Tarfaya Atlantic coastal Basin, SW Morocco, *Cretaceous Res.*, *45*, 288–305, doi:10.1016/j.cretres.2013.05.004.

Arthur, M. A., and B. B. Sageman (2004), Sea-level control on source-rock development: Perspectives from the Holocene Black Sea, the mid-Cretaceous Western Interior Basin of North America and the Late Devonian Appalachian Basin, in *The Deposition of Organic-Carbon-Rich Sediments: Models, Mechanisms, and Consequences*, *Spec. Publ*, vol. 82, edited by N. B. Harris, pp. 35–59, SEPM (Society for Sedimentary Geology), Tulsa, Okla.

Arthur, M. A., W. E. Dean, and L. M. Pratt (1988), Geochemical and climatic effects of increased marine organic-carbon burial at the Cenomanian-Turonian Boundary, *Nature*, *335*, 714–717, doi:10.1038/335714a0.

Barclay, R. S., J. C. McElwain, and B. B. Sageman (2010), Carbon sequestration activated by a volcanic CO_2 pulse during Ocean Anoxic Event 2, *Nat. Geosci.*, *3*, 205–208, doi:10.1038/NGEO757.

Batenburg, S. J., D. Vleeschouwer, M. Sprovieri, F. J. Hilgen, A. S. Gale, B. S. Singer, C. Koeberl, R. Coccioni, P. Claeys, and A. Montanari (2016), Orbital control on the timing of oceanic anoxia in the Late Cretaceous, *Clim. Past*, *12*, 1995–2009, doi:10.5194/cp-12-1995-2016. [Available at http://ww.clim-past.net/12/1995/2016/.]

Berger, W. H., L. Diester-Haass, and J. S. Killingley (1978), Upwelling off Northwest Africa: The Holocene decrease as seen in carbon isotopes and sedimentological indicators, *Oceanol. Acta*, *1*, 3–7.

Caron, M., S. Dall'Agnolo, H. Accarie, E. Barrera, E. G. Kauffman, F. Francis Amédro, and F. Robaszynski (2006), High-resolution stratigraphy of the Cenomanian–Turonian boundary interval at Pueblo (USA) and Wadi Bahloul (Tunisia): Stable isotope and bio-events correlation, *Geobios*, *39*, 171–200.

Choubert, G., A. Faure Muret, and L. Hottinger (1966), Aperçu géologique du Bassin côtier de Tarfaya (Stratigraphie), in *Le bassin côtier de Tarfaya (Maroc Méridional): Notes et Mémoire Service Géologique du Maroc*, vol. 175, edited by G. Choubert et al., pp. 7–106.

Clement, A. C., and L. C. Peterson (2008), Mechanisms of abrupt climate change of the last glacial period, *Rev. Geophys.*, *46*, RG4002, doi:10.1029/2006RG000204.

De Moel, H., G. M. Ganssen, F. J. C. Peeters, S. J. A. Jung, D. Kroon, G. J. A. Brummer, and R. E. Zeebe (2009), Planktic foraminiferal shell thinning in the Arabian Sea due to anthropogenic ocean acidification?, *Biogeosciences*, *6*, 1917–1925. [Available at http://www.biogeosciences.net/6/1917/2009/.]

Dean, W. E., M. A. Arthur, and G. E. Claypool (1986), Depletion of 13C in Cretaceous marine organic matter: Source, diagenetic, or environmental signal?, *Mar. Geol.*, *70*(1–2), 119–157, doi:10.1016/0025-3227(86)90092-7.

DeConto, R. M., S. Galeotti, M. Pagani, D. Tracy, K. Schaefer, T. Zhang, D. Pollard, and D. J. Beerling (2012), Past extreme warming events linked to massive carbon release from thawing permafrost, *Nature*, *484*, 87–91.

Desmares, D., D. Grosheny, and B. Beaudoin (2008), Ontogeny and phylogeny of upper Cenomanian rotaliporids (foraminifera), *Mar. Micropaleontol.*, *69*, 91–105, doi:10.1016/j.marmicro.2008.07.003.

Du Vivier, A. D. C., D. Selby, B. B. Sageman, D. R. Gröcke, and S. Voigt (2014), Osmium isotope dynamics during Cenomanian-Turonian OAE 2 reveal interplay of changing global seawater chemistry and circulation, *Earth Planet. Sci. Lett.*, *389*, 23–33.

Du Vivier, A. D. C., A. D. Jacobson, G. O. Lehn, D. Selby, M. T. Hurtgen, and B. B. Sageman (2015), Ca isotope stratigraphy across the Cenomanian–Turonian OAE 2: Links between volcanism, seawater geochemistry, and the carbonate fractionation factor, *Earth Planet. Sci. Lett.*, *416*, 121–131, doi:10.1016/j.epsl.2015.02.001.

El Khatib, J., E. Ruellan, A. El Foughali, and A. El Morabet (1995), Évolution de la marge atlantique sud-marocaine: Bassin de Tarfaya-Laâyoune, *C. R. Acad. Sci. Paris IIa*, *320*, 117–124.

El Khatib, J., A. El Foughali, E. Ruellan, and A. El Morabet (1996), Évolution post-rift des secteurs NE et SW du bassin Tarfaya-Laâyoune, *Mines. Géol. Energ.*, *55*, 57–72.

Elbatal, Y., M. Aadjour, N. Saber, R. Elabibi, and M. Nahim (2010), Étude sismo-structurale du basin de Tarfaya-Boujdour Onshore, *Afr. Sci.*, *06*(2), 49–59.

Elder, W. P., E. R. Gustason, and B. B. Sageman (1994), Correlation of basinal carbonate cycles to nearshore parasequences in the Late Cretaceous Greenhorn Seaway, Western Interior, USA, *Geol. Soc. Am. Bull.*, *106*, 892–902.

Elrick, M., R. Garza, R. Duncan, and L. Snow (2009), C-isotope stratigraphy and paleoenvironmental changes recorded in Cenomanian-Turonian (mid-Cretaceous) platform carbonates of southern Mexico, *Earth Planet. Sci. Lett.*, *277*, 295–306, doi:10.1016/j.epsl.2008.10.020.

Erbacher, J., O. Friedrich, P. A. Wilson, H. Birch, and J. Mutterlose (2005), Stable organic carbon isotope stratigraphy across oceanic anoxic event 2 of demerara rise, western tropical Atlantic, *Geochem. Geophys. Geosyst.*, *6*, Q06010, doi:10.1029/2004GC000850.

Erdem, Z., J. Schönfeld, N. Glock, M. Dengler, T. Mosch, S. Sommer, J. Elger, and A. Eisenhauer (2016), Peruvian sediments as recorders of an evolving hiatus for the last 22 thousand years, *Quat. Sci. Rev.*, *137*, 1–14, doi:10.1016/j.quascirev.2016.01.029.

Falkowski, P. G., R. T. Barber, and V. V. Smetacek (1998), Biogeochemical controls and feedbacks on ocean primary production, *Science*, *281*(5374), 200–206.

Flögel, S., K. Wallmann, and W. Kuhnt (2011), Cool episodes in the Cretaceous—Exploring the effects of physical forcings on Antarctic snow accumulation, *Earth Planet. Sci. Lett.*, *307*, 279–288, doi:10.1016/j.epsl.2011.04.024.

Gale, A. S., and W. K. Christensen (1996), Occurrence of the belemnite *Actinocamax plenus* in the Cenomanian of SE France and its significance, *Bull. Geol. Soc. Denmark*, *43*, 68–77.

Gale, A. S., J. Hardenbol, B. Hathway, W. J. Kennedy, J. R. Young, and V. Phansalkar (2002), Global correlation of Cenomanian (Upper Cretaceous) sequences: Evidence for Milankovitch control on sea level, *Geology*, *30*(4), 291–294.

Gertsch, B., T. Adatte, G. Keller, A. A. M. Tantawy, Z. Berner, H. P. Mort, and D. Fleitmann (2010), Middle and late Cenomanian oceanic anoxic events in shallow and deeper shelf environments of western Morocco, *Sedimentology*, *57*, 1430–1462, doi:10.1111/j.1365-3091.2010.01151.x.

Govin, A., U. Holzwarth, D. Heslop, L. Ford Keeling, M. Zabel, S. Mulitza, J. A. Collins, and C. M. Chiessi (2012), Distribution of major elements in Atlantic surface sediments (36°N–49°S): Imprint of terrigenous input and continental weathering, *Geochem. Geophys. Geosyst.*, *13*, 1–23, doi:10.1029/2011GC003785.

Grosheny, D., B. Beaudoin, L. Morel, and D. Desmares (2006), High-resolution biostratigraphy and chemostratigraphy of the Cenomanian/Turonian boundary event in the Vocontian Basin, Southern France, *Cretaceous Res.*, *27*, 629–640.

Haug, G. H., K. A. Hughen, D. M. Sigman, L. S. Peterson, and U. Röhl (2001), Southward migration of the Intertropical Convergence Zone through the Holocene, *Science*, *293*(5533), 1304–1308, doi:10.1126/science.1059725.

Hayes, J. M., H. Strauss, and A. J. Kaufman (1999), The abundance of 13C in marine organic matter and isotopic fractionation in the global biogeochemical cycle of carbon during the past 800 ma, *Chem. Geol.*, *161*, 103–125.

Higgins, J. A., and D. P. Schrag (2006), Beyond methane: Towards a theory for the Paleocene–Eocene thermal maximum, *Earth Planet. Sci. Lett.*, *245*, 523–537, doi:10.1016/j.epsl.2006.03.009.

Holbourn, A. E., W. Kuhnt, K. G. D. Kochhann, N. Andersen, and S. Meier (2015), Global perturbation of the carbon cycle at the onset of the Miocene Climatic Optimum, *Geology*, *43*, 123–126, doi:10.1130/G36317.1.

Houghton, R. A. (2007), Balancing the global carbon budget, *Annu. Rev. Earth Planet. Sci.*, *35*, 313–347.

Jarvis, I., A. S. Gale, H. C. Jenkyns, and M. A. Pearce (2006), Secular variation in late cretaceous carbon isotopes: A new δ13C carbonate reference curve for the Cenomanian–Campanian (99.6–70.6 ma), *Geol. Mag.*, *143*, 561–608, doi:10.1017/S0016756806002421.

Jarvis, I., J. S. Lignum, D. R. Gröcke, H. C. Jenkyns, and M. A. Pearce (2011), Black shale deposition, atmospheric CO_2 drawdown, and cooling during the Cenomanian-Turonian Oceanic Anoxic Event, *Paleoceanography*, *26*, PA3201, doi:10.1029/2010PA002081.

Jarvis, I., J. Trabucho-Alexandre, D. R. Gröcke, D. Ulicny, and J. Lurin (2015), Intercontinental correlation of organic carbon and carbonate stable isotope records: Evidence of climate and sea-level change during the Turonian (Cretaceous), *Depositional Rec.*, *1*(2), 53–90, doi:10.1002/dep2.6.

Jenkyns, H. C., A. J. Dickson, M. Ruhl, and S. H. J. M. Can den Boorn (2017), Basalt-seawater interaction, the Plenus Cold Event, enhanced weathering and geochemical change: Deconstructing OAE 2 (Cenomanian-Turonian, Late Cretaceous), *Sedimentology*, *64*, 16–43, doi:10.1111/sed.12305.

Kaiho, K., M. Katabuchi, M. Oba, and M. Lamolda (2014), Repeated anoxia–extinction episodes progressing from slope to shelf during the latest Cenomanian, *Gondwana Res.*, *25*(4), 1357–1368.

Kemp, A. E. S. (1996), Laminated sediments as palaeo-indicators, in *Palaeoclimatology and Palaeoceanography from Laminated Sediments*, edited by A.E.S. Kemp, *Geol. Soc. Spec. Publ.*, *116*, 7–12, doi:10.1144/GSL.SP.1996.116.01.01.

Kirtland Turner, S. (2014), Pliocene switch in orbital-scale carbon cycle/climate dynamics, *Paleoceanography*, *29*, 1256–1266, doi:10.1002/2014PA002651.

Kolonic, S., J. S. Sinninghe Damsté, M. E. Böttcher, M. M. M. Kuypers, W. Kuhnt, B. Beckmann, G. Scheeder, and T. Wagner (2002), Geochemical characterization of Cenomanian/Turonian black shales from the Tarfaya Basin (SW Morocco), *J. Pet. Geol.*, *25*, 325–350, doi:10.1111/j.1747-5457.2002.tb00012.x.

Kolonic, S., et al. (2005), Black shale deposition on the northwest African Shelf during the Cenomanian/Turonian oceanic anoxic event: Climate coupling and global organic carbon burial, *Paleoceanography*, *20*, 1–18, doi:10.1029/2003PA000950.
Kuhnt, W., J. Thurow, J. Wiedmann, and J. P. Herbin (1986), Oceanic anoxic conditions around the Cenomanian/Turonian Boundary and the response of the biota, in *Biogeochemistry of Black Shales*, vol. 60, edited by E. T. Degens, P. A. Meyers, and S. C. Brassell, pp. 205–246, Mitteilungen aus dem Geologischen Institut der Univ. Hamburg, Germany.
Kuhnt, W., J. P. Herbin, J. Thurow, and J. Wiedmann (1990), Distribution of Cenomanian-Turonian organic facies in the western Mediterranean and along the adjacent Atlantic margin, in *Deposition of Organic Facies*, *Am. Assoc. Pet. Geol. Stud. Geol*, vol. 30, edited by A. Y. Huc, pp. 133–160.
Kuhnt, W., A. Nederbragt, and L. Leine (1997), Cyclicity of Cenomanian-Turonian organic-carbon-rich sediments in the Tarfaya Atlantic Coastal Basin (Morocco), *Cretaceous Res.*, *18*, 587–601, doi:10.1006/cres.1997.0076.
Kuhnt, W., et al. (2001), Morocco Basin's sedimentary record may provide correlations for Cretaceous paleoceanographic events worldwide, *Eos Trans. AGU*, *82*(33), 361–364.
Kuhnt, W., F. Luderer, S. Nederbragt, J. Thurow, and T. Wagner (2005), Orbital-scale record of the late Cenomanian-Turonian oceanic anoxic event (OAE-2) in the Tarfaya Basin (Morocco), *Int. J. Earth Sci.*, *94*, 147–159, doi:10.1007/s00531-004-0440-5.
Kuhnt, W., A. Holbourn, A. Gale, E. H. Chellai, and W. J. Kennedy (2009), Cenomanian sequence stratigraphy and sea-level fluctuations in the Tarfaya Basin (SW Morocco), *Bull. Geol. Soc. Am.*, *121*, 1695–1710, doi:10.1130/B26418.1.
Kuhnt, W., A. Holbourn, and M. Moullade (2011), Transient global cooling at onset of early Aptian Anoxic Event (OAE1a), *Geology*, *39*(4), 323–326, doi:10.1130/G31554.1.
Kump, L. R., and M. A. Arthur (1999), Interpreting carbon-isotope excursions: Carbonates and organic matter, *Chem. Geol.*, *161*, 181–198.
Kuroda, J., N. Ohkouchi, T. Ishii, H. Tokuyama, and A. Taira (2005), Lamina-scale analysis of sedimentary components in Cretaceous black shales by chemical compositional mapping: Implications for paleoenvironmental changes during the Oceanic Anoxic Events, *Geochim. Cosmochim. Acta*, *69*(6), 1479–1494.
Küspert, W. (1982), Environmental change during oil shale deposition as deduced from stable isotope ratios, in *Cyclic and Event Stratification*, edited by S. Einsele and A. Seilacher, pp. 482–501, Springer, New York.
Kuypers, M. M. M., R. D. Pancost, I. A. Nijenhuis, and J. S. Sinninghe Damsté (2002), Enhanced productivity led to increased organic carbon burial in the euxinic North Atlantic basin during the late Cenomanian oceanic anoxic event, *Paleoceanography*, *17*(4), 1051, doi:10.1029/2000PA000569.
Larson, R. L., and E. Erba (1999), Onset of the mid-Cretaceous greenhouse in the Barremian-Aptian: Igneous events and the biological, sedimentary, and geochemical responses, *Paleoceanography*, *14*, 663–678, doi:10.1029/1999PA900040.
Laskar, J., P. Robutel, F. Joutel, M. Gastineau, A. C. M. Correia, and B. Levrard (2004), A long term numerical solution for the insolation quantities of the Earth, *Astron. Astrophys.*, *428*, 261–285.
Laskar, J., A. Fienga, M. Gastineau, and H. Manche (2011), La2010: A new orbital solution for the long-term motion of the Earth, *Astron. Astrophys.*, *532*(A89), 1–15.
Laurin, J., and B. B. Sageman (2007), Cenomanian-Turonian coastal record in SW Utah, U.S.A.: Orbital-scale transgressive-regressive events during Oceanic Anoxic Event II, *J. Sediment. Res.*, *77*, 731–756, doi:10.2110/jsr.2007.076.
Laurin, J., S. R. Meyers, D. Uličný, I. Jarvis, and B. B. Sageman (2015), Axial obliquity control on the greenhouse carbon budget through middle- to high-latitude reservoirs, *Paleoceanography*, *30*, 133–149, doi:10.1002/2014PA002736.
Laws, E. A., B. N. Popp, R. R. Bidigare, M. C. Kennicutt, and S. A. Macko (1995), Dependence of phytoplankton carbon isotope composition on growth rate and (CO_2)aq: Theoretical considerations and experimental results, *Geochim. Cosmochim. Acta*, *59*, 1131–1138.
Leine, L. (1986), Geology of the Tarfaya oil shale deposit, Morocco, *Geol. Mijnbouw*, *65*, 57–74.
Li, X., H. C. Jenkyns, C. Wang, X. Hu, C. Xi, Y. Wei, Y. Huang, and C. Jie (2006), Upper Cretaceous carbon- and oxygen-isotope stratigraphy of hemipelagic carbonate facies from southern Tibet, China, *J. Geol. Soc., London*, *163*, 375–382.
Locklair, R. E., and B. B. Sageman (2008), Cyclostratigraphy of the Upper Cretaceous Niobrara Formation, western interior, U.S.A.: A Coniacian–Santonian orbital timescale, *Earth Planet. Sci. Lett.*, *269*, 539–552.
Longoria, J. F. (1973), *Pseudoticinella*, a new genus of planktonic foraminifera from the early Turonian of Texas, *Rev. Española Micropaleontol.*, *5*, 417–423.
Lorenzen, J., W. Kuhnt, A. Holbourn, S. Flögel, M. Moullade, and G. Tronchetti (2013), A new sediment core from the Bedoulian (Lower Aptian) stratotype at Roquefort-La Bédoule, SE France, *Cretaceous Res.*, *39*, 6–16, doi:10.1016/j.cretres.2012.03.019.
Luderer, F., and W. Kuhnt (1997), A high resolution record of the *Rotalipora* extinction in laminated organic-carbon rich limestones of the Tarfaya Atlantic coastal basin (Morocco), *Ann. Soc. Géol. Nord (2eme Sér.)*, *5*, 199–205.
Ma, C., S. Meyers, B. Sageman, B. Singer, and B. Jicha (2014), Testing the astronomical time scale for oceanic anoxic event 2, and its extension into Cenomanian strata of the Western Interior Basin, *Geol. Soc. Am. Bull.*, *126*, 974–989.
Meyers, P. A. (2014), Why are the δ^{13}C org values in Phanerozoic black shales more negative than in modern marine organic matter? *Geochem. Geophys. Geosyst.*, *15*, 3085–3106, doi:10.1002/2014GC005305.
Meyers, P. A., S. M. Bernasconi, and A. Forster (2006), Origins and accumulation of organic matter in expanded Albian to Santonian black shale sequences on the Demerara Rise, South American margin, *Org. Geochem.*, *37*, 1816–1830.
Meyers, S. R., B. B. Sageman, and M. A. Arthur (2012a), Obliquity forcing of organic matter accumulation during Oceanic Anoxic Event 2, *Paleoceanography*, *27*, 1–19, doi:10.1029/2012PA002286.
Meyers, S. R., S. E. Siewert, B. S. Singer, B. B. Sageman, D. J. Condon, J. D. Obradovich, B. R. Jicha, and D. A. Sawyer (2012b), Intercalibration of radioisotopic and astrochonologic time scales for the Cenomanian-Turonian boundary interval, Western Interior Basin, USA, *Geology*, *40*, 7–10, doi:10.1130/G32261.1.
Mort, H. P., T. Adatte, G. Keller, D. Bartels, K. B. Föllmi, P. Steinmann, Z. Berner, and E. H. Chellai (2008), Organic carbon deposition and phosphorus accumulation during Oceanic Anoxic Event 2 in Tarfaya, *Morocco: Cretaceous Res.*, *29*, 1008–1023, doi:10.1016/j.cretres.2008.05.026.
Mosch, T., S. Sommer, M. Dengler, A. Noffke, L. Bohlen, O. Pfannkuche, V. Liebetrau, and K. Wallmann (2012), Factors influencing the distribution of epibenthic megafauna across the Peruvian oxygen minimum zone, *Deep Sea Res., Part I*, *168*, 123–135, doi:10.1016/j.dsr.2012.04.014.
Mulitza, S., M. Prange, J.-B. Stuut, M. Zabel, T. von Dobeneck, A. C. Itambi, J. Nizou, M. Schulz, and G. Wefer (2008), Sahel megadroughts triggered by glacial slowdowns of Atlantic meridional overturning, *Paleoceanography*, *23*, PA4206, doi:10.1029/2008PA001637.
Nederbragt, A., and A. Fiorentino (1999), Stratigraphy and palaeoceanography of the Cenomanian–Turonian boundary event in Oued Mellegue, north-western Tunisia, *Cretaceous Res.*, *20*, 47–62.
Paul, C. R. C., M. A. Lamolda, S. F. Mitchell, M. R. Vaziri, A. Gorostidi, and J. D. Marshall (1999), The Cenomanian–Turonian boundary at Eastbourne (Sussex, UK): A proposed European reference section, *Palaeogeogr. Palaeoclimatol. Palaeoecol.*, *150*, 83–121.
Peterson, L. C., G. Haug, K. A. Hughen, and U. Röhl (2000), Rapid changes in the hydrologic cycle of the tropical Atlantic during the last glacial, *Science*, *290*, 1947–1951, doi:10.1126/science.290.5498.1947.

Ranke, U., U. Von Rad, and G. Wissman (1982), Stratigraphy, facies and tectonic development of the On- and Offshore Aaiun-Tarfaya Basin, in *Geology of the Northwest African Continental Margin*, edited by U. von Rad et al., pp. 87–105, Springer, Heidelberg.

Ratschiller, L. K. (1970), Lithostratigraphy of the northern Spanish Sahara, *Mem. Mus. Tridentino Sci. Trento*, *18*(1), 1–80.

Rothwell, R. G., and I. W. Croudace (2015), Twenty years of XRF core scanning marine sediments: What do geochemical proxies tell us?, in *Micro-XRF Studies of Sediment Cores*, edited by I. W. Croudace and R. G. Rothwell, *Dev. Paleoenviron. Res*., vol. 17, pp. 25–102, doi:10.1007/978-94-017-9849-5_2, Springer, Dordrecht, Netherlands.

Ryan, W. B. F., et al. (2009), Global multi-resolution topography synthesis, *Geochem. Geophys. Geosyst.*, *10*, Q03014, doi:10.1029/2008GC002332.

Sageman, B. B. (1996), Lowstand tempestites: Depositional model for Cretaceous skeletal limestones, Western Interior basin, *Geology*, *24*(10), 888–892.

Sageman, B. B., S. R. Meyers, and M. A. Arthur (2006), Orbital time scale and new C-isotope record for Cenomanian- Turonian boundary stratotype, *Geology*, *34*, 125–128.

Sames, B., et al. (2016), Review: Short-term sea-level changes in a greenhouse world—A view from the Cretaceous, *Palaeogeogr. Palaeoclimatol. Palaeoecol.*, *441*(2016), 393–411.

Schönfeld, J., W. Kuhnt, Z. Erdem, S. Flögel, N. Glock, M. Aquit, M. Frank, and A. Holbourn (2015), Records of past mid-depth ventilation: Cretaceous ocean anoxic event 2 vs. recent oxygen minimum zones, *Biogeosciences*, *12*(4), 1169–1189, doi:10.5194/bg-12-1169-2015.

Stoll, H. M. (2005), Limited range of interspecific vital effects in coccolith stable isotopic records during the Paleocene-Eocene thermal maximum, *Paleoceanography*, *20*, PA1007, doi:10.1029/2004PA001046.

Storey, M., R. A. Duncan, and C. C. Swisher (2007), Paleocene-Eocene thermal maximum and the opening of the northeast Atlantic, *Science*, *316*(5824), 587–589.

Tessin, A., I. Hendy, N. Sheldon, and B. B. Sageman (2015), Redox-controlled preservation of organic matter during "OAE 3" within the Western Interior Seaway, *Paleoceanography*, *30*, 702–717, doi:10.1002/2014PA002729.

Timmermann, A., S. J. Lorenz, S.-I. An, A. Clement, and S.-P. Xie (2007), The effect of orbital forcing on the mean climate and variability of the tropical Pacific, *J. Clim.*, *20*, 4147–4159, doi:10.1175/JCLI4240.1.

Tisserand, A., B. Malaizé, E. Julien, S. Zaragosi, K. Charlier, and F. Grousset (2009), Ti African monsoon enhancement during the penultimate glacial period (MIS 6.5 ~170 ka) and its atmospheric impact, *Paleoceanography*, *24*, PA2220, doi:10.1029/2008PA001630.

Tsikos, H., et al. (2004), Carbon isotope stratigraphy recorded by the Cenomanian–Turonian Oceanic Anoxic Event: Correlation and implications based on three key localities, *J. Geol. Soc.*, *161*, 711–719.

Turgeon, S. C., and R. A. Ceaser (2008), Cretaceous oceanic anoxic event 2 triggered by a massive magmatic episode, *Nature*, *454*, 323–326.

van Bentum, E. C., G. J. Reichart, A. Forster, and J. S. Sinninghe Damsté (2012), Latitudinal differences in the amplitude of the OAE-2 carbon isotopic excursion: pCO_2 and paleoproductivity, *Biogeosciences*, *9*, 717–731, doi:10.5194/bg-9-717-2012.

Van Helmond, N. A. G. M., A. Sluijs, G. J. Reichart, J. S. Sinninghe Damsté, C. P. Slomp, and H. Brinkhuis (2014), A perturbed hydrological cycle during Oceanic Anoxic Event 2, *Geology*, *42*, 123–126.

Voigt, S., J. Erbacher, J. Mutterlose, W. Weiss, T. Westerhold, F. Wiese, M. Wilmsen, and T. Wonik (2008), The Cenomanian–Turonian of the Wunstorf section (north Germany): Global stratigraphic reference section and new orbital time scale for oceanic anoxic event 2, *Newsl. Stratigr.*, *43*, 65–89.

Wagreich, M., R. Lein, and B. Sames (2014), Eustasy, its controlling factors, and the limnoeustatic hypothesis—Concepts inspired by Eduard Suess, *Aust. J. Earth Sci.*, *107*, 115–131.

Weltje, G. J., and R. Tjallingii (2008), Calibration of XRF core scanners for quantitative geochemical logging of sediment cores: Theory and application, *Earth Planet. Sci. Lett.*, *274*, 423–438, doi:10.1016/j.epsl.2008.07.054.

Wendler, I. (2013), A critical evaluation of carbon isotope stratigraphy and biostratigraphic implications for late cretaceous global correlation, *Earth Sci. Rev.*, *126*, 116–146.

Wendler, J. E., and I. Wendler (2016), What drove sea-level fluctuations during the mid-Cretaceous greenhouse climate? *Palaeogeogr. Palaeoclimatol. Palaeoecol.*, *441*, 412–419.

Wendler, J. E., I. Wendler, and B. T. Huber (2013), Revision and evaluation of the systematic affinity of the Calcitarch genus Pithonella based on exquisitely preserved Turonian material from Tanzania, *J. Paleontol.*, *87*(6), 1077–1106, doi:10.1666/12-121.

Wiedmann, J., A. Butt, and G. Einsele (1978), Vergleich von marokkanischen Kreide-Küstenaufschlüssen und Tiefseebohrungen (DSDP): Stratigraphie, Paläoenvironment und Subsidenz an einem passiven Kontinentalrand, *Geol. Rundsch.*, *67*, 454–508, doi:10.1007/BF01802800.

Wiedmann, J., A. Butt, and G. Einsele (1982), Cretaceous stratigraphy, environment, and subsidence history at the Moroccan continental margin, in *Geology of the Northwest African Continental Margin*, edited by U. von Rad et al., pp. 366–395, Springer, Berlin.

Zachos, J. C., H. McCarren, B. Murphy, U. Röhl, and T. Westerhold (2010), Tempo and scale of late Paleocene and early Eocene carbon isotope cycles: Implications for the origin of hyperthermals, *Earth Planet. Sci. Lett.*, *299*(1–2), 242–249, doi:10.1016/j.epsl.2010.09.004.